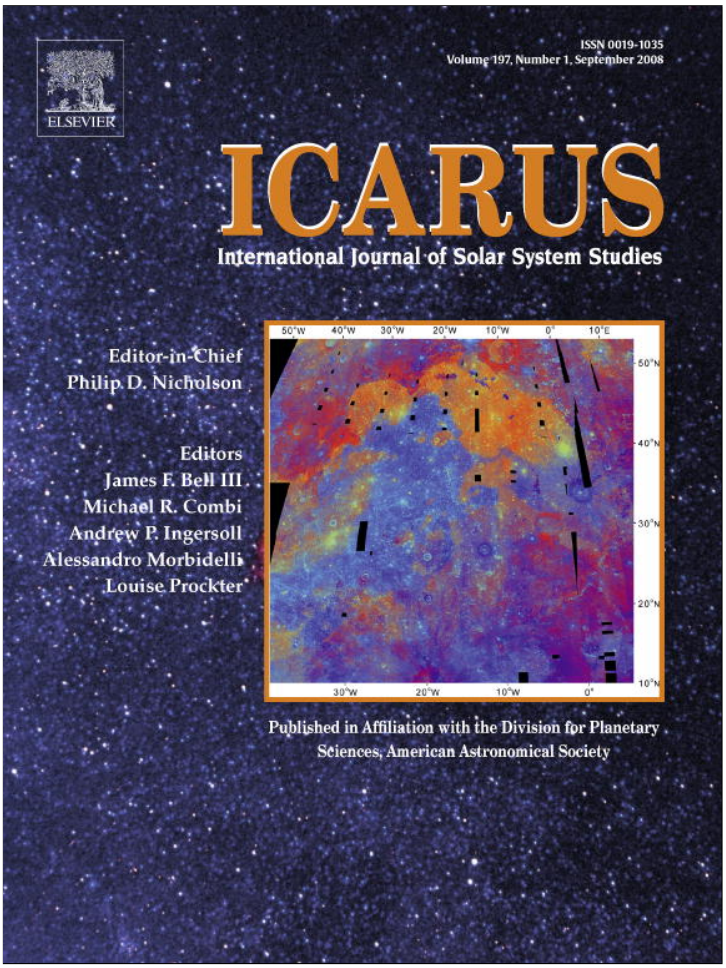

Icarus 197 (2008) 110–136

Contents lists available at ScienceDirect

Icarus

www.elsevier.com/locate/icarus

Coupled ion and neutral rotating model of Titan's upper atmosphere

V. De La Haye [a], J.H. Waite Jr. [a,*], T.E. Cravens [b], I.P. Robertson [b], S. Lebonnois [c]

[a] Southwest Research Institute, 6220 Culebra, PO Drawer 28510, San Antonio, TX 78228-0510, USA
[b] Department of Physics and Astronomy, University of Kansas, Lawrence, KS 66045, USA
[c] Laboratoire de Meteorologie Dynamique, Jussieu, 75252 Paris, France

ARTICLE INFO

Article history:
Received 14 August 2007
Revised 27 March 2008
Available online 10 April 2008

Keywords:
Titan
Atmospheres, chemistry
Photochemistry

ABSTRACT

A one-dimensional composition model of Titan's upper atmosphere is constructed, coupling 36 neutral species and 47 ions. Energy inputs from the Sun and from Saturn's magnetosphere and updated temperature and eddy coefficient parameters are taken into account. A rotating technique at constant latitude and varying local-time is proposed to account for the diurnal variation of solar inputs. The contributions of photodissocation, neutral chemistry, ion–neutral chemistry, and electron recombination to neutral production are presented as a function of altitude and local time. Local time-dependent mixing ratio and density profiles are presented in the context of the T_A and T_5 Cassini data and are compared in detail to previous models. An independent and simplified ion and neutral scheme (19-species) is also proposed for future 3D-purposes. The model results demonstrate that a complete understanding of the chemistry of Titan's upper atmosphere requires an understanding of the coupled ion and neutral chemistry. In particular, the ionospheric chemistry makes significant contributions to production rates of several important neutral species.

1. Introduction

Titan's complex ion and neutral chemistry is initiated by the ionization and dissociation of nitrogen and methane, energized by solar photons or magnetospheric electrons, resulting in a great variety of heavy hydrocarbons and nitriles. Many photochemical models were developed during the last twenty years in attempts to describe this complex chemistry. Following the encounter of Titan by Voyager 1 in November 1981, Yung et al. (1984) and Yung (1987) outlined the major chemical mechanisms, and constructed a photochemical model that would be used as a basis for the subsequent models (Toublanc et al., 1995; Lara et al., 1996). Following the study of Toublanc et al. (1995), a 2D-model (latitude/altitude) was developed by Lebonnois et al. (2001) between 0 and 1240 km, by coupling the general circulation model of Hourdin et al. (1995) with the photochemical scheme of Toublanc et al. (1995). The photochemical scheme used in Lebonnois et al. (2001) was updated in further 1D studies (Lebonnois et al., 2003; Lebonnois, 2005), and the vertical eddy diffusion coefficient was adjusted below 500 km to account for meridional mixing by general circulation.

The first general circulation model of Titan's upper atmosphere ($z > 600$ km) was reported in Müller-Wodarg et al. (2000) and Müller-Wodarg and Yelle (2002), taking into account solar radiation and vertical coupling with middle atmosphere winds. Müller-Wodarg et al. (2003) then used the GCM of Müller-Wodarg et al. (2000) to calculate the global distribution of neutral gases due to wind and diffusion in the upper atmosphere.

The strong dependence of the ionosphere on the background neutral atmosphere was underscored by Keller et al. (1992), Fox and Yelle (1997), and Keller et al. (1998). The construction of the first coupled ion–neutral composition models followed (Banaszkiewicz et al., 2000; Wilson and Atreya, 2004). In particular, Wilson and Atreya (2004) performed a sensitivity study on the eddy coefficient, obtaining a best fit for the Voyager data with a homopause at 850 km and a methane mole fraction of 2.2% in the stratosphere.

In the afore-mentioned composition models, the neutral temperature profiles were chosen as fixed parameters determined after the first analysis of the UVS Voyager data by Smith et al. (1982) and the subsequent studies of Strobel et al. (1992) and Yelle et al. (1997). These studies suggested an exospheric temperature of 175 ± 30 K and the presence of a mesopause at $\simeq$565 km with a temperature of $\simeq$135 K. Recently, however, the reanalysis of the UVS Voyager data by Vervack et al. (2004) and the analysis of the first INMS Cassini data (De La Haye et al., 2007a; Waite et al., 2005; Yelle et al., 2006) suggested an asymptotic temperature about 20 to 30 K lower, and questioned the presence of a mesopause. Such a difference in temperature profiles mainly affects the components' scale heights, an essential component in the diffusion equation, and to a lesser extent the reaction rates.

* Corresponding author. Fax: +1 210 543 0052.
E-mail address: hwaite@swri.edu (J.H. Waite Jr.).

0019-1035/$ – see front matter
doi:10.1016/j.icarus.2008.03.022

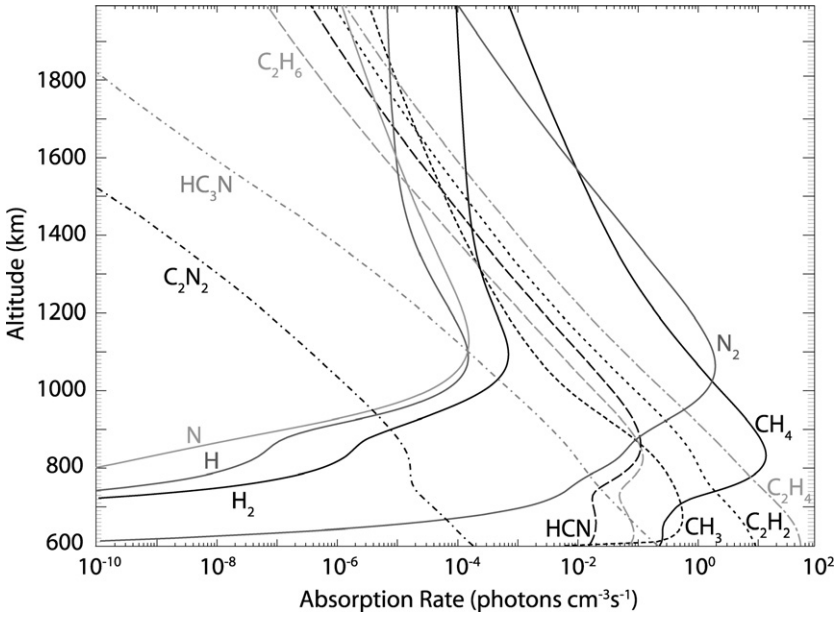

Fig. 1. Comparison of solar radiation absorption rate at zenith angle 60° for neutrals present in Titan's upper atmosphere.

Taking these considerations into account, the construction of a new one-dimensional composition model is presented. The model describes interdependent ion and neutral densities for altitudes between 600 and 2000 km, and includes the dissociation and ionization schemes of the atmospheric neutrals by incoming solar photons and magnetospheric electrons. A rotating method is developed allowing for the study of local time variations at constant latitude, and providing a quasi-two-dimensional approach to the modeling. The ion and neutral density profiles resulting from this local time-dependent model are presented for the latitudinal and solar conditions of the first close Titan flybys by the Cassini Orbiter: T_A in October 2004 and T_5 in April 2005. Both flybys took place on Titan's wake side with respect to Saturn's magnetosphere.

2. Construction of the ion–neutral rotating model

Titan's complex ion and neutral chemistry is initiated by the impact of photons and electrons on molecular nitrogen, methane, and major hydrocarbons. The solar fluxes impinging on Titan's upper atmosphere are determined using the EUVAC Solar Flux Model of Richards et al. (1994) and the method of Tobiska and Barth (1990) with the average radio fluxes $F_{Av}10.7$ cm = 106 s.f.u. for T_A and $F_{Av}10.7$ cm = 86 s.f.u. for T_5 (NOAA, 2005). Nitrogen is by far the dominant constituent (≃98%), and is the almost exclusive absorber of photons with energy in its absorption band, 16–1000 Å. Methane (≃2%) has a wider wavelength absorption band (16–1450 Å), and absorbs most photons in the remaining 1000–1450 Å wavelength range. The less energetic photons penetrate deeper into the atmosphere and can be absorbed by minor species such as C_2H_2, C_2H_4, C_2H_6, and HC_3N (Fig. 1). The photoelectron and magnetospheric electron fluxes are determined separately using the model of Gan et al. (1992), with parabolic magnetospheric field lines and conditions corresponding to the magnetospheric wake. The photo- and electron-impact-absorption cross sections and related dissociation and ionization quantum yields are referenced in Table 1. When they were available, values corresponding to Titan's temperatures (≃150 K) were selected.

The model includes 35 neutral species: H, H_2, C, CH, $^3CH_2$, $^1CH_2$, CH_3, CH_4, C_2, C_2H, C_2H_2, C_2H_3, C_2H_4, C_2H_5, C_2H_6, C_3H_3, CH_3C_2H, $CH_2C_2H_2$, C_3H_8, C_4H_2, c-C_6H_6, l-C_6H_6, N(^4S), N(^2D), N(^2P), N_2, NH, CN, HCN, H_2CN, C_2N, C_2N_2, HC_3N, HC_3N^*, and Ar. The neutral–neutral chemical reactions are selected from the model of Wilson and Atreya (2004) and that of Lebonnois et al. (2001), updated in Lebonnois et al. (2003) and Lebonnois (2005). Vertical transport is modeled using the diffusion equation presented in Yelle et al. (2006) and De La Haye et al. (2007a), recast from its more classic form to take into account minor and major species, and especially CH_4's non-negligible density compared to N_2. With the same considerations, molecular diffusion was described for a multicomponent gas (Wilke, 1950; Wilson and Atreya, 2004), using N_2–s and CH_4–s binary coefficients from Banks and Kockarts (1973), Wakeham and Slater (1973), and Mason and Marrero (1970), or derived using the study of Wilson and Atreya (2004) and Wilson (2002).

In a study of the INMS data recorded during flyby T_A, Yelle et al. (2006) found that certain combinations of eddy diffusion and upward flux of methane allow appropriate fit of the CH_4 density data. They found an eddy coefficient of $K \simeq 4 \times 10^9$ cm^2 s^{-1}, assuming a negligible CH_4 escape flux, and of $K \simeq 10^7$ cm^2 s^{-1}, assuming a CH_4 escape flux of 2.2×10^9 cm^{-2} s^{-1}, referred to Titan's surface. In the present study, the escape flux of methane was assumed to be negligible. A constant eddy coefficient of 4×10^9 cm^2 s^{-1} was considered in the upper part of the atmosphere (De La Haye et al., 2007a), a value in good agreement with the effective eddy diffusion coefficient calculated in Müller-Wodarg and Yelle (2002), including the effects of horizontal dynamics. Below ≃1200 km, the eddy coefficient profile was assumed to decrease with decreasing altitude, reaching 5×10^7 cm^2 s^{-1} at 600 km, following the contour of the effective eddy diffusion coefficient of Müller-Wodarg and Yelle (2002).

Two neutral temperature profiles, corresponding to flybys T_A and T_5, are built and used as fixed inputs to the present model. Above 1025 km, isothermal profiles of 152.8 and 157.4 K are assumed, based on the fit of the T_A and T_5 INMS data (De La Haye et al., 2007a). A temperature of 182 K is chosen at 300 km, midway between the value of the engineering model of Yelle et al. (1997) and the value from the CIRS data analyzed by Flasar et al. (2005). Simple interpolations were made between the two altitude regions, and hydrostatic equilibrium was verified. The temperature profiles are plotted in Fig. 2 and compared to the T_A UVIS results of Shemansky et al. (2005). A characteristic of the Shemansky et al. (2005) profile stands in the presence of a cold mesopause with a value of 115 K at 600 km. According to our calculations, how-

Table 1
References used for the ionization and dissociation cross sections

Species	Photoabsorption cross section	Photodissociation quantum yield	Photoionization quantum yield	Electron impact cross section
H		← Schunk and Nagy (2000) →		Wilson (2002) Shah et al. (1987)
H_2		← Schunk and Nagy (2000) →		Wilson (2002) Backx et al. (1976)
CH_4	16–50 Å: Gan (1991), Lukirskii et al. (1964) 50–1050 Å: Schunk and Nagy (2000) 1050–1200 Å: Hudson (1971) 1200–1400 Å: Chen and Wu (2004) 1400–1600 Å: Mount et al. (1977)	Wilson (2002) Romani (1996)	16–50 Å: Gan (1991) Lukirskii et al. (1964) 50–1050 Å: Schunk and Nagy (2000)	Wilson (2002) Orient and Srivastava (1987)
C_2H_2	Wilson (2002) 150–750 Å: Wu and Judge (1985) 750–1200 Å: Cooper et al. (1995) 1200–2100 Å: Wu et al. (2001) 2100–2300 Å: Seki and Okabe (1993)	1100–1650 Å: Okabe (1981) 1650–1900 Å: Okabe (1983) 1900–2300 Å: Seki and Okabe (1993) Reviewed with: Vuitton et al. (2006a) Läuter et al. (2002)	16–650 Å: Zheng and Srivastava (1996)	Wilson (2002) Zheng and Srivastava (1996)
C_2H_4	Wilson (2002) Holland et al. (1997) Zelikoff and Wanabee (1953) Schmitt and Brehm (1966)	Wilson (2002) Chang et al. (1998)	16–700 Å: Tian and Vidal (1998a)	Wilson (2002) Tian and Vidal (1998a)
C_2H_6	Wilson (2002) Au et al. (1993) Mount and Moos (1978)	Wilson (2002) Mount et al. (1977) Kameta et al. (1996)	16–700 Å: Tian and Vidal (1998b) 700–1050 Å: Wilson (2002) Kameta et al. (1996)	Wilson (2002) Tian and Vidal (1998b)
$N(^4S)$	Wilson (2002) Fenelly and Torr (1992)			Wilson (2002) Brook et al. (1978)
N_2		16–50 Å: Stolte et al. (1998) ← 50–1000 Å: Schunk and Nagy (2000) →		Wilson (2002) Zipf et al. (1980) Itikawa et al. (1986)
HCN		Wilson (2002) ← Nuth and Glicker (1982) → Kreile et al. (1982)		Keller et al. (1992) same as C_2H_2
HC_3N	Wilson (2002) Connors et al. (1974) Clarke and Ferris (1996) Andrieux et al. (1995) Bénilan et al. (1994) Bruston et al. (1989)	Clarke and Ferris (1995) Halpern et al. (1988)		
C_2N_2		← Clarke and Ferris (1995) → Halpern et al. (1988)		Not modeled

ever, there appears to be incompatibility between the Shemansky et al. (2005) temperature profile, and the verification of hydrostatic equilibrium between the CIRS density data at 300 km (Flasar et al., 2005) and the INMS density data above 1174 km (Waite et al., 2005). As mentioned in the introduction, the Yung et al. (1984), Toublanc et al. (1995), and Wilson and Atreya (2004) models used earlier temperature profiles, based on the first analyses of the Voyager ingress UVS data by Smith et al. (1982): a 174 K-isothermal profile in Yung et al. (1984), the temperature profile recommended by Lellouch and Hunten (1987) in Toublanc et al. (1995), and the temperature profile recommended by Yelle et al. (1997) in Wilson and Atreya (2004). The model of Lebonnois et al. (2001) was recently re-run for altitudes above 500 km, a latitude of 40° N, and a season corresponding to the winter solstice. This new run used the updated chemistry and eddy diffusion coefficient of Lebonnois et al. (2003) and Lebonnois (2005) and the temperature profile suggested by Vervack et al. (2004) after the re-analysis of the Voyager ingress UVS data.

Compared to the models of Yung et al. (1984), Toublanc et al. (1995), Wilson and Atreya (2004), and Lebonnois (2005), which describe Titan's atmosphere from the surface to altitudes close to the exobase, the present model focuses on the upper atmosphere and

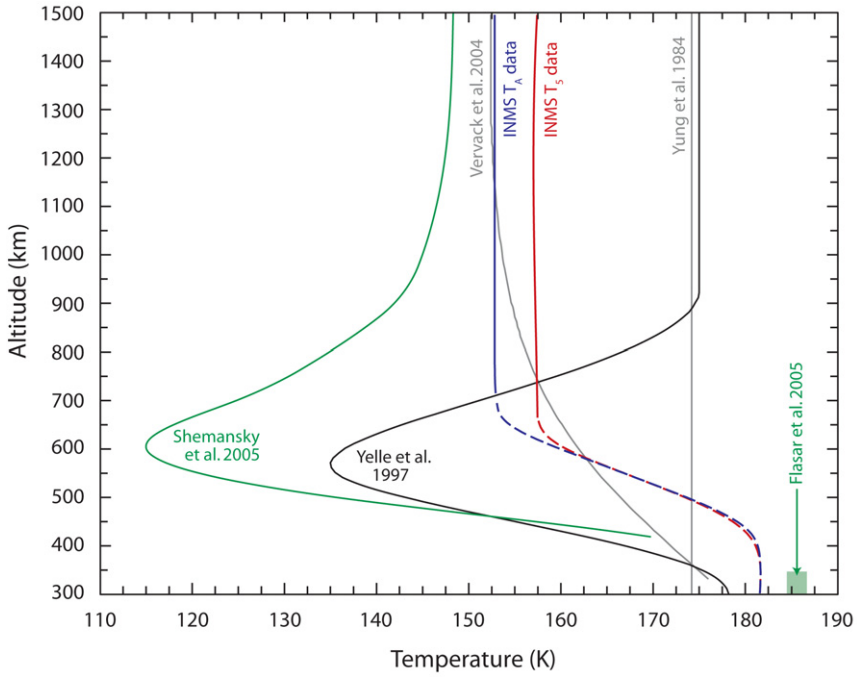

Fig. 2. Temperature profiles derived from the Cassini INMS (De La Haye et al., 2007a), CIRS (Flasar et al., 2005) and UVIS (Shemansky et al., 2005) data, and from the analysis (Smith et al., 1982; Yelle et al., 1997) and revised analysis (Vervack et al., 2004) of the Voyager UVS data. The profiles noted 'INMS T_A data' and 'INMS T_5 data,' extended by dash lines, were used as inputs into the present coupled ion–neutral rotating model.

exosphere between 600 and 2000 km. At 600 km, the mixing ratios are assumed to be fixed for all species with a lifetime larger than one percent of a Titan rotational period (for example species N_2, CH_4, H_2, C_2H_2, C_2H_4, C_2H_6, C_3H_4, and Ar). For species with shorter lifetimes, for example C_2H or $N(^4S)$, photochemical equilibrium is assumed as the boundary condition. Considering the afore-mentioned set of input parameters (temperature and eddy coefficient), the lower boundary mixing ratios of the present model are adjusted at 600 km to match adequately the INMS density data recorded at higher altitudes. If no INMS data are available, the mixing ratios are taken directly from the Lebonnois (2005) results at 600 km.

The exobase, defined here as the altitude at which atmospheric scale height and mean free path are equal, constitutes the upper limit of the collisional region. The altitude of the exobase is recalculated after each time iteration, assuming a common exobase for all species except H_2 and H. For these two lighter species, the exobase is found at $\simeq$1700 km, about 300 km higher than other species. Once the exobase altitude is determined, a collisional regime is modeled below, taking into account chemistry and vertical transport, and exospheric processes are modeled above, using a method based on the Liouville theorem (De La Haye et al., 2007a; Schunk and Nagy, 2000). In the present model, as in the models of Yung et al. (1984), Toublanc et al. (1995), Wilson and Atreya (2004), and Lebonnois (2005), the upper boundary condition of the collisional region is set in terms of an escape flux. Thermal escape fluxes (Jeans escape) are applied and are found to be significant for H_2 and H but negligible for all other species.

The ionospheric model is constructed using the model of Keller et al. (1992, 1998). Photoequilibrium is assumed. A few ion–neutral and electron recombination rates were updated using Anicich (2003), Kella et al. (1996), Lehfaoui et al. (1997), Janev and Reiter (2004), and Sheehan and St-Maurice (2004). The electron temperature profile is chosen as that reported by Wahlund et al. (2005) for inbound T_A. The model includes the following 44 ions: H^+, H_2^+, H_3^+, C^+, CH^+, CH_2^+, CH_3^+, CH_4^+, CH_5^+, C_2H^+, $C_2H_2^+$, $C_2H_3^+$, $C_2H_4^+$, $C_2H_5^+$, $C_2H_6^+$, C_3H^+, c-$C_3H_2^+$, l-$C_3H_3^+$, c-$C_3H_3^+$, $C_3H_4^+$, $C_3H_5^+$, $C_3H_6^+$, $C_3H_7^+$, $C_4H_2^+$, $C_4H_3^+$, $C_4H_5^+$, $C_4H_7^+$, $C_5H_3^+$, $C_5H_5^+$, $C_5H_7^+$, $C_5H_9^+$, $C_6H_7^+$, $C_7H_7^+$, N^+, N_2^+, NH^+, N_2H^+, CN^+, HCN^+, H_2CN^+, CNC^+, C_3HN^+, $C_3H_2N^+$, and $C_5H_5N^+$. As in Keller et al. (1998), three additional species are taken into account: $C_{n\geqslant 2}H_{m^+}$ representing other hydrocarbon ions, and ZLO^+ and ZHI^+ representing nitrile ions with mass lower and greater than 30 amu, respectively. Our model does not include some of the new ion species observed by the Cassini INMS (e.g., masses 18 and 30 as suggested in Cravens et al., 2006, identified as NH_4^+ and $CH_2NH_2^+$ in Vuitton et al., 2006b), but it does couple the ion and neutral chemistry and provide insight into the formation of key hydrocarbon species as a function of local time.

The idea of a one-dimensional rotating model, sweeping through a range of zenith angles from day to night and from night to day, is introduced to take into account the diurnal variation effects, such as the ceasing of the solar flux induced mechanisms on the night side. For coupling purposes, it is interesting to note the relative time scale of the modeled processes. The time constants corresponding to molecular diffusion ($\tau_{D_s} = H_s^2/D_s$), eddy diffusion ($\tau_K = H_a^2/K$), and ion and neutral chemistry ($\tau_{\mathrm{chem},s} = -\frac{(\partial n_s/\partial t)_{\mathrm{loss}}}{n_s}$) are plotted in Fig. 3 and compared to Titan's rotational period, $\tau_{\mathrm{Titan}} \simeq 16$ Earth days. Ion chemistry is found to be several orders of magnitude faster than a Titan day, as opposed to neutral chemistry and diffusion, which are found to be slower or comparable to τ_{Titan}. Ion mechanisms are therefore considered instantaneous, whereas time iterations are taken into account for neutral processes. An estimate of the thermal structure time constant, τ_T, based on the calculation of the HCN rotational cooling rate, is also included in Fig. 3. This shows that the time scales of Titan's thermal structure are comparable to Titan's rotational period. Thermal structure variations, however, are judged to be beyond the scope of the present paper, and a temperature profile that is constant with local time is assumed throughout the study.

The rotating method is operated by dividing each Titan day into twelve local time sectors (Fig. 4). The latitude is fixed to 38.8° N for T_A and 73.7° N for T_5. Subsequently, using a subsolar latitude value of 23° S, the zenith angles corresponding to

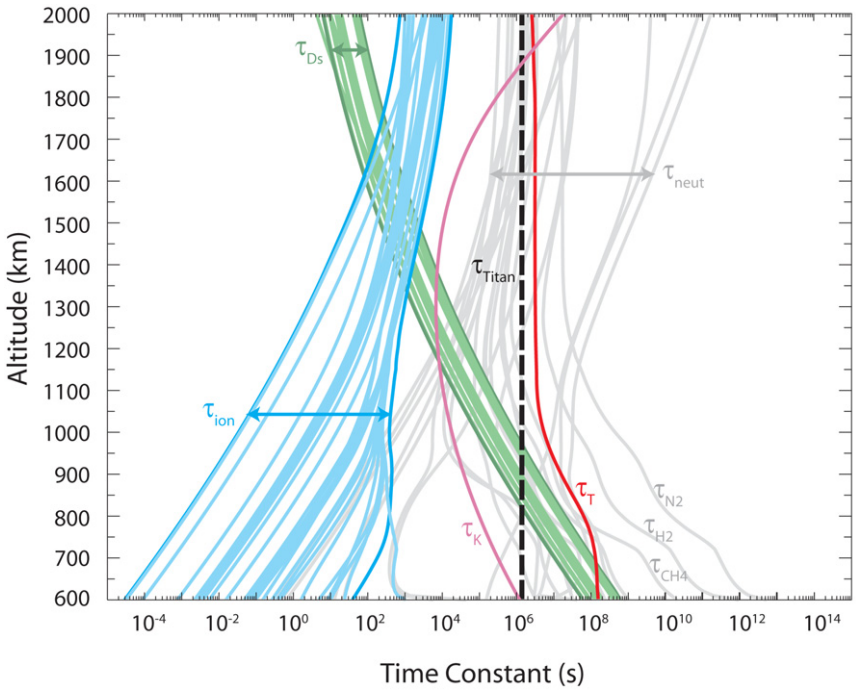

Fig. 3. Comparison of the time constants in Titan's upper atmosphere. τ_{neut} (in grey) are the chemistry time constants for the neutrals (e.g. τ_{N_2}, τ_{CH_4} and τ_{H_2} correspond to the chemical life time of nitrogen, methane and hydrogen), τ_{D_s} (in green) are the molecular diffusion time constants, τ_K (in pink) the eddy diffusion time constant, τ_{ion} (in blue) the time constants for the ions, and τ_T (in red) the thermal structure time constant. These parameters are compared to Titan's rotational period, τ_{Titan} (black dash line).

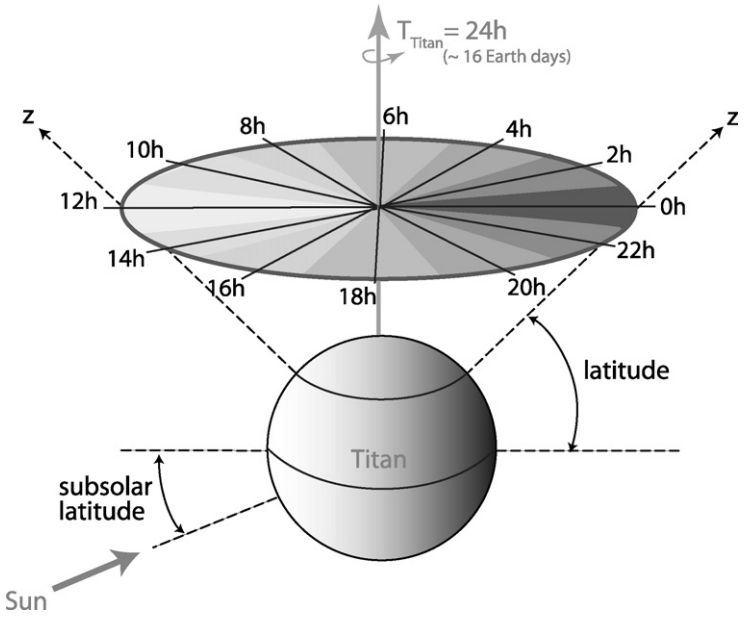

Fig. 4. Illustration of the rotating model: division of the two-dimensional space with constant latitude into local time sectors.

the twelve local time sectors were determined to vary between 61.7° at noon and 164.8° at midnight in the T_A conditions, and between 97.0° at noon and 129.0° at midnight in the T_5 conditions. Within each local time sector, the zenith angle and therefore the solar and electron fluxes, are assumed to be constant. After each Titan day, the neutral density profiles corresponding to the sectors' centers are compared to those of the previous rotation until periodic equilibrium is reached (10 to 14 Titan days). The solar flux and ion density profiles are re-calculated once and twice, respectively, per local time sector. The fluxes of photo- and magnetospheric electrons were computed independently using the model of Gan et al. (1992). Considering that Titan's orbit around Saturn is synchronous, particles in Titan's atmosphere remain in the same configuration with respect to Saturn over time. The flux of magnetospheric electrons was therefore assumed to be constant with local time, and conditions corresponding to the magnetospheric wake were chosen to match the T_A and T_5 closest approach configurations. For the calculation of the photo-electron flux, several runs were performed using Gan et al. (1992) to cover the necessary range of zenith angles.

The possibility of the atmospheric particles rotating at a slightly different speed than Titan's surface is also considered, using the longitudinal component of the wind calculated in Müller-Wodarg et al. (2000) averaged over the altitude range 600–1450 km. The

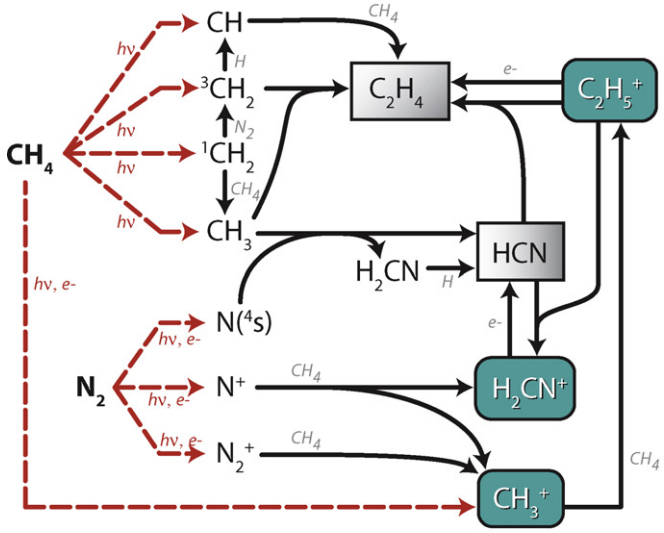

Fig. 5. Chemical scheme I. Construction of the first key neutrals and ions starting from photon and electron impact with nitrogen and methane: C_2H_4, HCN, H_2CN^+, $C_2H_5^+$, and CH_3^+.

number of time steps per sector is modified so that particles remain longer in sectors with lower angular velocity and pass faster through sectors with higher angular velocity. In particular, it is noted that particles are submitted about 5 times longer to morning radiation ($\simeq$6 h) than to afternoon radiation ($\simeq$18 h).

3. Local time-dependent ion–neutral production

The ion and neutral chemical mechanisms that take place in Titan's upper atmosphere are studied as a function of local time with a particular emphasis on the role played by ion–neutral processes. Considering the extent of the number of species and reactions involved, local time-dependent production rate profiles are only presented for a few species, C_2H_2, C_2H_4, C_2H_6, C_3H_4, and C_6H_6, most of them initially observed by INMS (Waite et al., 2005). More complete discussion of all species is found in De La Haye et al. (2007b) and De La Haye (2005).

3.1. Ethylene and the primary ion–neutral chemical processes

The formation of C_2H_4 is the first important step in the foundation of Titan's upper atmospheric chemistry (Fig. 5). The first of the two main production paths follows the photodissociation of methane into reactive species CH, $^3CH_2$, $^1CH_2$, and CH_3. [The same C_2H_4 production scheme was used in Lebonnois (2005) and Wilson and Atreya (2004).]

$$CH_4 + h\nu \rightarrow CH,\ {}^3CH_2,\ {}^1CH_2,\ CH_3,$$

$${}^1CH_2 + N_2 \rightarrow {}^3CH_2 + N_2,$$

$${}^1CH_2 + CH_4 \rightarrow CH_3 + CH_3,$$

$${}^3CH_2 + H \rightarrow CH + H_2,$$

$$CH + CH_4 \rightarrow C_2H_4 + H,$$

$${}^3CH_2 + CH_3 \rightarrow C_2H_4 + H. \quad (1)$$

Different methane photodissociation schemes were proposed by Mordaunt et al. (1993), Romani (1996), and Smith and Raulin (1999). While the study of Mordaunt et al. (1993) was experimental, using an adaptation of the technique of $H(D)$ photofragment translational spectroscopy, the two other studies were mostly based on models and constraints from previous experiments. In Romani (1996), the branching ratio leading to $^1CH_2 + H + H$ was arbitrarily set to zero, leading to an overdetermined system of constraints then solved with a least-squares fit method. Sensitivity studies of the methane photodissociation scheme on Titan's atmospheric composition were performed in Wilson and Atreya (1999) and Lebonnois (2000). In particular, Lebonnois (2000) focused on the consequence of different amounts of $^1CH_2$ released into the atmosphere, and found that the only noticeable effect appeared in the mixing ratio of $CH_2C_2H_2$. In the present study, the photodissociation scheme chosen in Wilson and Atreya (2004), i.e. the scheme of Romani (1996), was selected.

The second C_2H_4 production path follows the photo- and electron impact dissociation and ionization of nitrogen (Wilson, 2002; Schunk and Nagy, 2000; Stolte et al., 1998; Itikawa et al., 1986; Zipf et al., 1980), either involving the formation of key ions CH_3^+ and $C_2H_5^+$ and the electron recombination of $C_2H_5^+$ through the following process:

$$N_2 + h\nu, e^- \rightarrow N_2^+, N^+ + N,$$

$$N_2^+ + CH_4 \rightarrow CH_3^+ + N_2 + H,$$

$$N^+ + CH_4 \rightarrow CH_3^+ + NH,$$

$$CH_4 + h\nu, e^- \rightarrow CH_3^+ + H,$$

$$CH_3^+ + CH_4 \rightarrow C_2H_5^+ + H_2,$$

$$C_2H_5^+ + e^- \rightarrow C_2H_4 + H, \quad (2)$$

or involving the formation of HCN followed by ion–neutral chemistry:

$$CH_4 + h\nu \rightarrow CH_3 + H,$$

$$N_2 + h\nu, e^- \rightarrow N(^4s) + \cdots,$$

$$N(^4s) + CH_3 \rightarrow H_2CN + H,$$

$$H_2CN + H \rightarrow HCN + H_2,$$

$$C_2H_5^+ + HCN \rightarrow C_2H_4 + H_2CN^+. \quad (3)$$

In the altitude range of the present study ($z > 600$ km), the termolecular mechanism leading to the production of C_2H_4 through $C_2H_3 + H \xrightarrow{M} C_2H_4$ was found to be negligible by about four orders of magnitude compared to the afore-mentioned processes.

The altitude-dependent influence of the ethylene production mechanisms are compared in Fig. 6 for various local times. These profiles were computed using the T_A solar and latitudinal conditions, taking into account the effects of both photo- and magnetospheric electrons. On the day side, ethylene production is dominated by neutral chemistry processes [Eq. (1)] below 1045 km, by ion–neutral chemistry [Eq. (2)] between 1045 and 1400 km, and by electron recombination [Eq. (3)] above 1400 km. On the night side, neutral chemistry is prevalent below 1100 km, and the peak production of C_2H_4 occurs higher, between 1100 and 1285 km, in the region where ion–neutral chemistry dominates. Above this region, ethylene is mainly produced by electron recombination.

Local time-dependent production rate profiles were plotted in Fig. 7 for hydrogen cyanide (HCN), a key neutral species for determining the thermal structure of Titan's upper atmosphere. Below $\simeq$1100 km, the production of HCN is found to be dominated by neutral chemistry [Eq. (3)], with production peaks of $\simeq 5.1 \times 10^1$ cm^3 s^{-1} at $\simeq$920 km on the day side, and $\simeq$9.9 cm^3 s^{-1} at $\simeq$830 km on the night side. Above 1100 km, the HCN production is found to be dominated by the electron recombination of H_2CN^+:

$$H_2CN^+ + e^- \rightarrow HCN + H. \quad (4)$$

It is interesting to note that the production mechanisms of HCN and H_2CN^+ are tightly related, with the main production mechanism of H_2CN^+ being $C_2H_5^+ + HCN \rightarrow C_2H_4 + H_2CN^+$ [Eq. (3)].

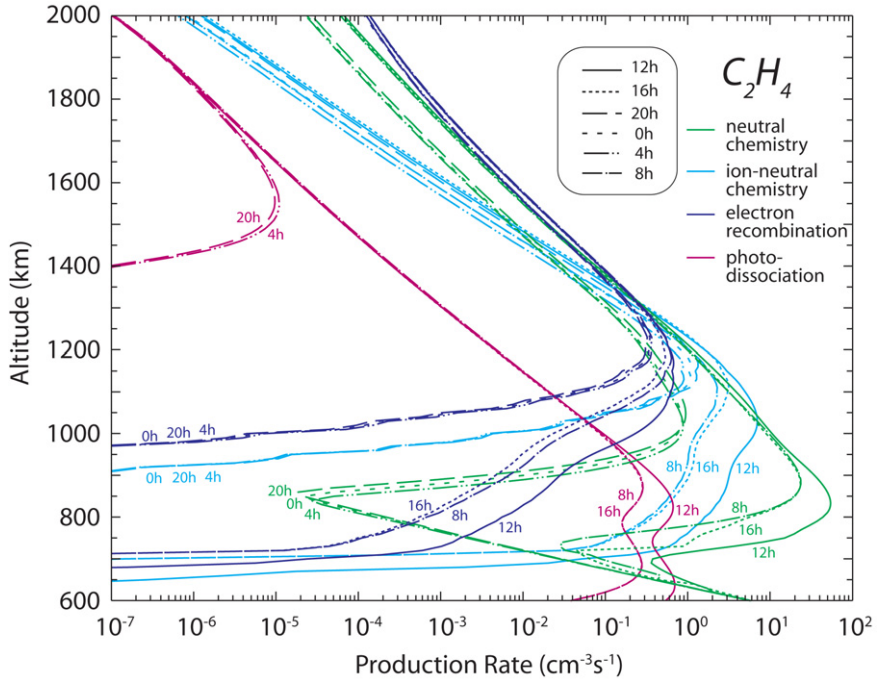

Fig. 6. Local time-dependent production rate profiles for C_2H_4, as computed by the present model for the T_A solar conditions, at a latitude of 38° North.

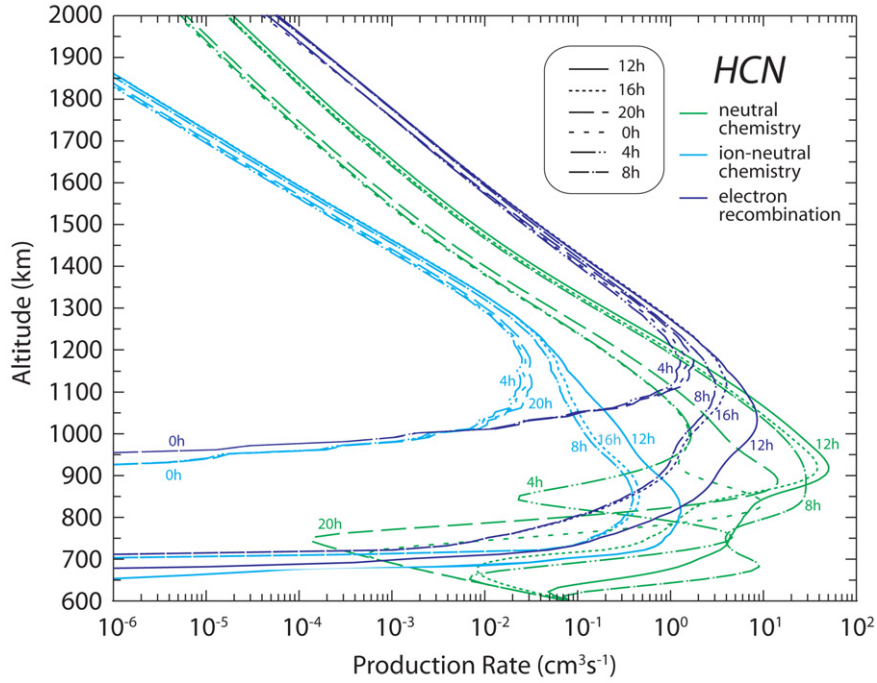

Fig. 7. Local time-dependent production rate profiles for HCN, as computed by the present model for the T_A solar conditions, at a latitude of 38° North.

The chemical species presented in Fig. 5 may be used to construct a self-sustainable ion and neutral composition model of Titan's upper atmosphere. All the species included in this scheme are presented with their most efficient production and loss mechanisms, with the addition of $CH_3 + CH_3 \xrightarrow{M} C_2H_6$ to model adequately the loss of CH_3 at low altitudes (see following section). This chemical scheme is also interesting in that it involves H_2CN^+ and $C_2H_5^+$, the two most abundant ions in Titan's ionosphere. The diurnally-averaged profiles obtained using the species of the simplified chemical scheme [i.e. neutrals H, H_2, CH, $^1CH_2$, $^3CH_2$, CH_3, CH_4, C_2H_4, N_2, $N(^4S)$, $N(^2D)$, $N(^2P)$, HCN, and H_2CN, and ions CH_3^+, $C_2H_5^+$, N^+, N_2^+, and H_2CN^+] and forcing all other species to zero are presented in Fig. 8. The results show good agreement with those obtained using the full ion and neutral scheme. The main discrepancy is found in an over-estimate of the H_2CN^+ profile at altitudes <900 km, due to the absence of $H_2CN^+ + C_4H_2 \rightarrow C_4H_3^+ + HCN$ from the simplified scheme. This process is, on average, about one order of magnitude less efficient than the electron recombination of H_2CN^+ [Eq. (4)], but it becomes the dominant loss process of H_2CN^+ at altitudes <900 km. Overall, the simplified chemical scheme is shown to constitute a good description of Titan's ion and neutral chemistry, and may be useful to future three dimensional models, considering their constraint of having a limited number of ion and neutral species.

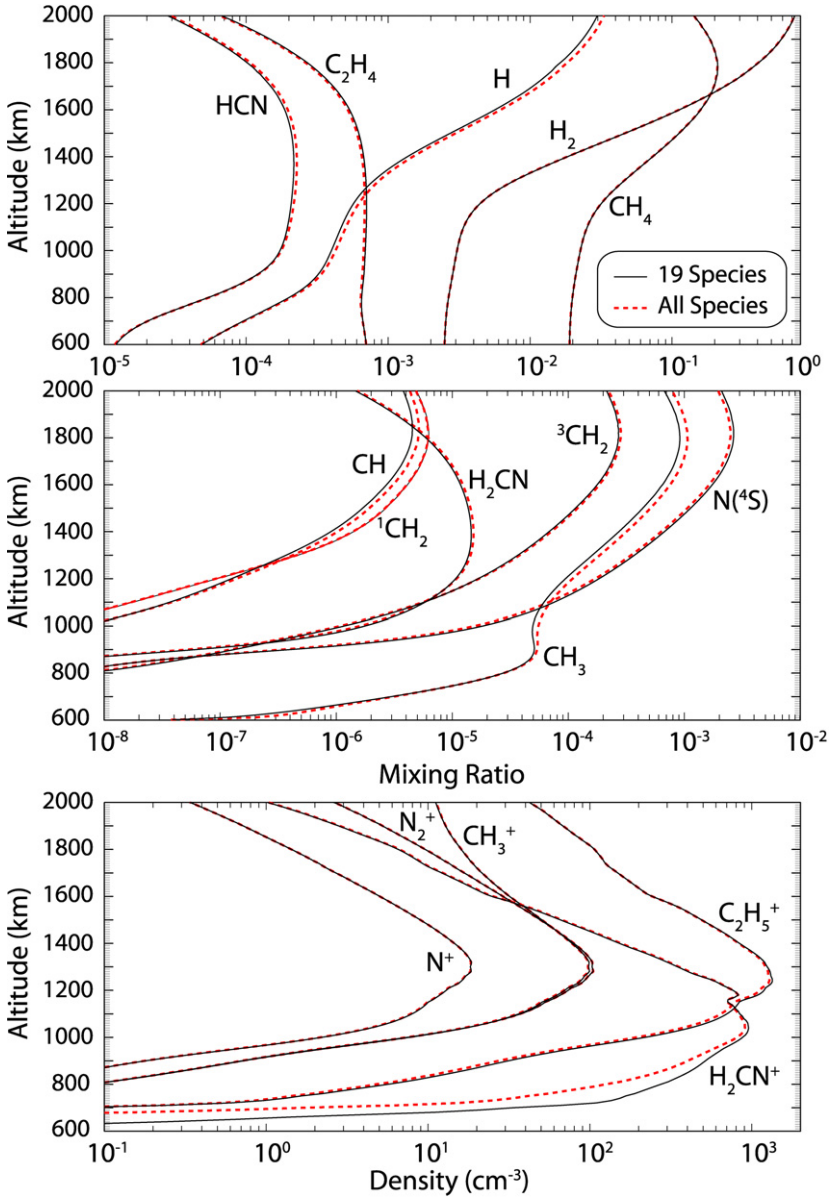

Fig. 8. Comparison of the diurnally-averaged composition profiles obtained when using the full chemical scheme involving 36 neutrals and 47 ions (dash red lines), and the independent and simplified 19 species-scheme, involving neutrals H, H_2, CH, $^1CH_2$, $^3CH_2$, CH_3, CH_4, C_2H_4, N_2, $N(^4S)$, $N(^2D)$, $N(^2P)$, HCN, and H_2CN, and ions CH_3^+, $C_2H_5^+$, N^+, N_2^+, and H_2CN^+ (solid black lines). The results are computed for the T_A solar conditions, at a latitude of 38° North.

3.2. Acetylene, ethane, and the second ion–neutral chemical processes

Now that C_2H_4 and $C_2H_5^+$ are formed, the complex formation of a series of hydrocarbons can begin. The chain of chemical reactions starts with the production of species such as C_2H_2, CH_3 and $C_3H_7^+$, and leads to the production of ethane and species as heavy as propane and diacetylene (Fig. 9).

Acetylene is essentially produced according to two processes. The first involves the photodissociation of ethylene,

$$C_2H_4 + h\nu \rightarrow C_2H_2 + H_2, \tag{5}$$

and the second the electron recombination of $C_2H_5^+$,

$$\begin{aligned} C_2H_5^+ + e^- &\rightarrow C_2H_2 + H_2 + H, \\ &\rightarrow C_2H_2 + 3H. \end{aligned} \tag{6}$$

Two additional processes insure the regeneration of acetylene after its photodissociation:

$$\begin{aligned} &C_2H_2 + h\nu \rightarrow C_2H + H, \\ &C_2H + C_2H_4 \rightarrow C_2H_2 + C_2H_3, \\ &C_2H + CH_4 \rightarrow C_2H_2 + CH_3, \end{aligned} \tag{7}$$

and

$$\begin{aligned} &C_2H_2 + h\nu \rightarrow C_2H + H, \\ &C_2H + H \xrightarrow{M} C_2H_2. \end{aligned} \tag{8}$$

Diacetylene is then produced as a result of the following reaction, involving the two newly created molecules C_2H_2 and C_2H:

$$C_2H_2 + C_2H \rightarrow C_4H_2 + H. \tag{9}$$

The production rate profiles of acetylene were plotted in Fig. 10. On the day side, production is dominated by ethylene photodissociation below 1035 km, Eq. (5), and by electron recombination

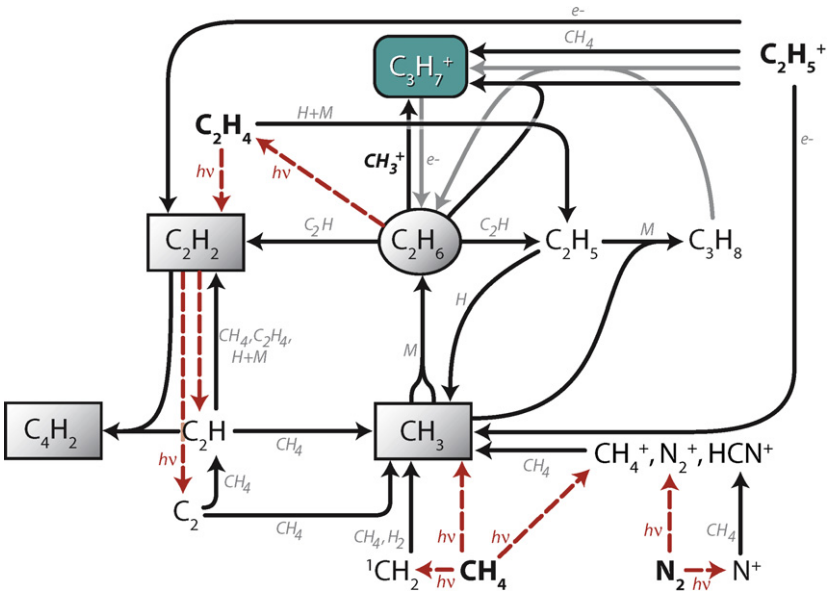

Fig. 9. Chemical scheme II. Production of key hydrocarbons: CH_3, C_2, C_2H, C_2H_2, C_2H_5, C_2H_6, C_3H_8, and C_4H_2, and related production of the ion $C_3H_7^+$. Species in bold are formed in previous chemical mechanisms.

above 1035 km, Eq. (6). On the night side, solar-driven mechanisms disappear, and neutral chemistry becomes prevalent below 1070 km. The C_2H_2 production by Eqs. (7) and (8) becomes insignificant below 815 km due to reactive species C_2H (mainly produced by acetylene photodissociation) being greatly depleted at low altitudes, where collision probability is higher. The termolecular process that appears below 815 km in Fig. 10 is due to $C_3H_4 + H \xrightarrow{M} CH_3 + C_2H_2$, which requires the production of C_3H_4 detailed in the next section. Ion–neutral mechanisms dominate the C_2H_2 night-side production rate over a short altitude range, between 1025 and 1100 km, essentially due to $C_2H_3^+ + HCN \rightarrow H_2CN^+ + C_2H_2$ and $C_2H_3^+ + C_2H_4 \rightarrow C_2H_5^+ + C_2H_2$ (see next section). Electron recombination [Eq. (6)] takes over above 1100 km.

The production of the minor species C_2H_6 is dominated between 600 and 900 km by the termolecular reaction:

$$CH_3 + CH_3 \xrightarrow{M} C_2H_6. \tag{10}$$

Above 900 km for the day side and above 1000 km for the night side, the production of ethane becomes dominated by ion–neutral chemistry below 1460 km, and electron recombination above 1460 km, both involving ion $C_3H_7^+$:

$$C_2H_5^+ + C_3H_8 \rightarrow C_2H_6 + C_3H_7^+, \tag{11}$$

$$C_3H_7^+ + e^- \rightarrow C_2H_6 + CH. \tag{12}$$

The C_2H_6 production rate profiles corresponding to these mechanisms are plotted in Fig. 11.

3.3. Methylacetylene and ion–neutral processes involving heavy hydrocarbons

The chemical processes leading to the production of methylacetylene (C_3H_4) and benzene (C_6H_6) are centered on the formation of C_3H_3 and involve ions CH_5^+, $C_2H_3^+$, $C_3H_5^+$ and $C_6H_7^+$, as described in Fig. 12. The major production mechanisms of methylacetylene (CH_3C_2H) and its reactive isomer ($CH_2C_2H_2$) are:

$$C_2H_4 + CH \rightarrow CH_3C_2H + H,$$
$$\rightarrow CH_2C_2H_2 + H, \tag{13}$$

and

$$C_3H_3 + H \xrightarrow{M} CH_3C_2H,$$
$$\xrightarrow{M} CH_2C_2H_2, \tag{14}$$

where the production of C_3H_3 is dominated by neutral chemistry below 900/1000 km on the day/night side,

$$C_2H_2 + {}^1CH_2 \rightarrow C_3H_3 + H, \tag{15}$$

and by electron recombination above,

$$C_2H_5^+ + C_2H_4 \rightarrow C_3H_5^+ + CH_4,$$

$$C_3H_5^+ + e^- \rightarrow C_3H_3 + H_2. \tag{16}$$

The following process then operates as a switch from the unstable to the stable isomer:

$$CH_2C_2H_2 + H \rightarrow CH_3C_2H + H. \tag{17}$$

The electron recombination of $C_3H_5^+$ also becomes the prevalent production process for methylacetylene above 950/1060 km on the day/night side (Fig. 13):

$$C_3H_5^+ + e^- \rightarrow CH_3C_2H + H. \tag{18}$$

The tight ion and neutral coupling involved in Titan's upper atmosphere is also important in the formation of benzene. Two main processes are responsible for its production: neutral chemistry below 700 km, involving the linear form of C_6H_6 as an intermediate,

$$C_3H_3 + C_3H_3 \xrightarrow{M} l\text{-}C_6H_6,$$

$$l\text{-}C_6H_6 + H \rightarrow c\text{-}C_6H_6 + H, \tag{19}$$

and electron recombination above 700 km, considering the preliminary formation of $C_4H_3^+$ and $C_6H_7^+$,

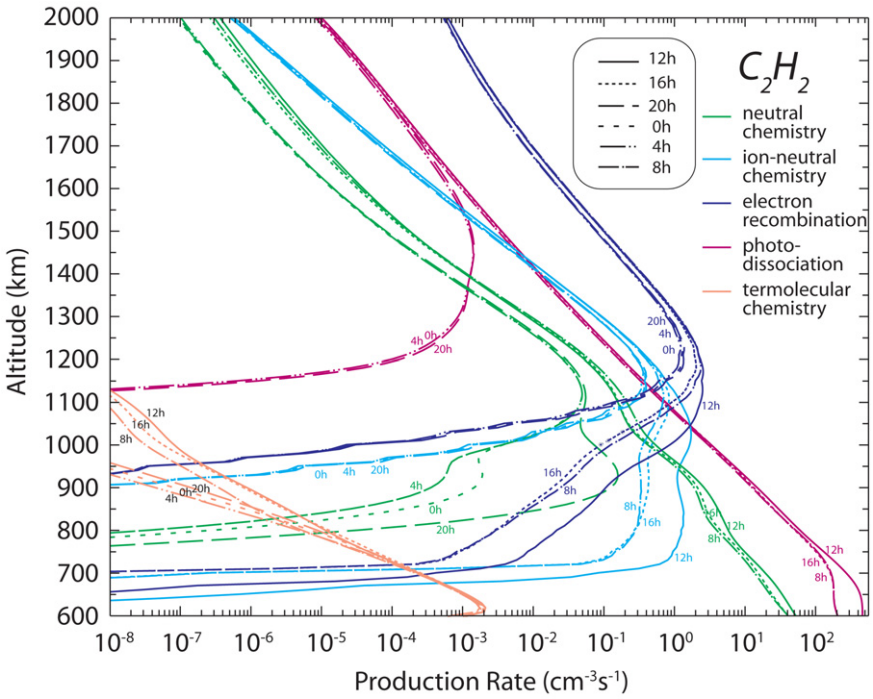

Fig. 10. Local time-dependent production rate profiles for C_2H_2, as computed by the present model for the T_A solar conditions, at a latitude of 38° North.

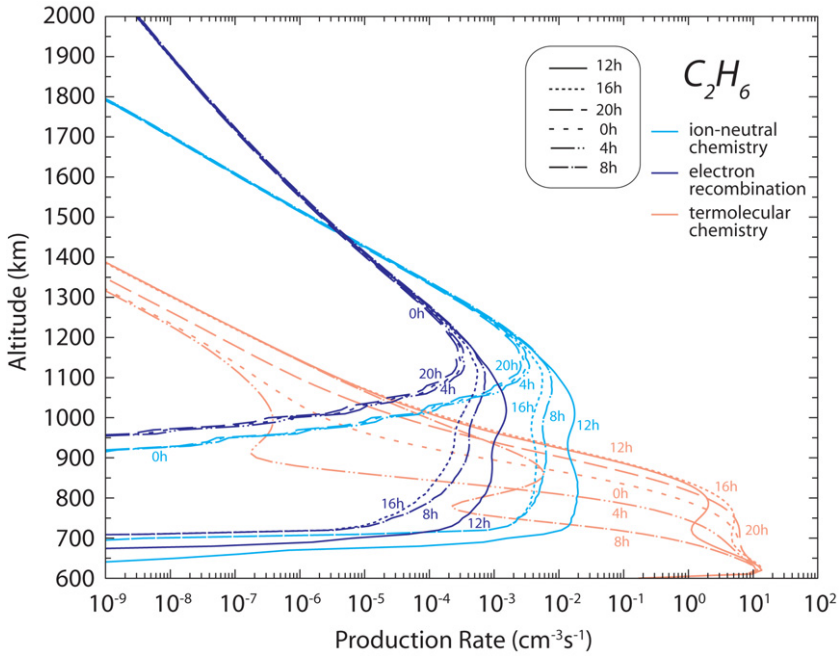

Fig. 11. Local time-dependent production rate profiles for C_2H_6, as computed by the present model for the T_A solar conditions, at a latitude of 38° North.

$$H_2CN^+ + C_4H_2 \rightarrow C_4H_3^+ + HCN,$$

$$C_4H_3^+ + C_2H_4 \rightarrow C_6H_7^+,$$

$$C_6H_7^+ + e^- \rightarrow c\text{-}C_6H_6 + H. \quad (20)$$

The production rate profile of benzene was plotted in Fig. 14. The peak production is found at 820 km on the day side and 1060 km on the night side, in the altitude region where Eq. (20) dominates. The c-C_6H_6-production due to ion–neutral chemistry in Fig. 14 is essentially due to $C_6H_7^+ + CH_3C_2H \rightarrow C_3H_5^+ + c\text{-}C_6H_6$. This mechanism is minor compared to Eq. (20) and is not indicated in the reaction scheme of Fig. 12.

3.4. Other nitriles

The cyano radical, CN, is the cornerstone of the nitrile chemistry scheme. It is produced through a variety of mechanisms including the participation of hydrogen cyanide. As shown in Fig. 15, heavier nitrile species, such as cyanoacetylene (HC_3N), CNC-radical (C_2N), and cyanogen (C_2N_2), are then produced by neutral–neutral

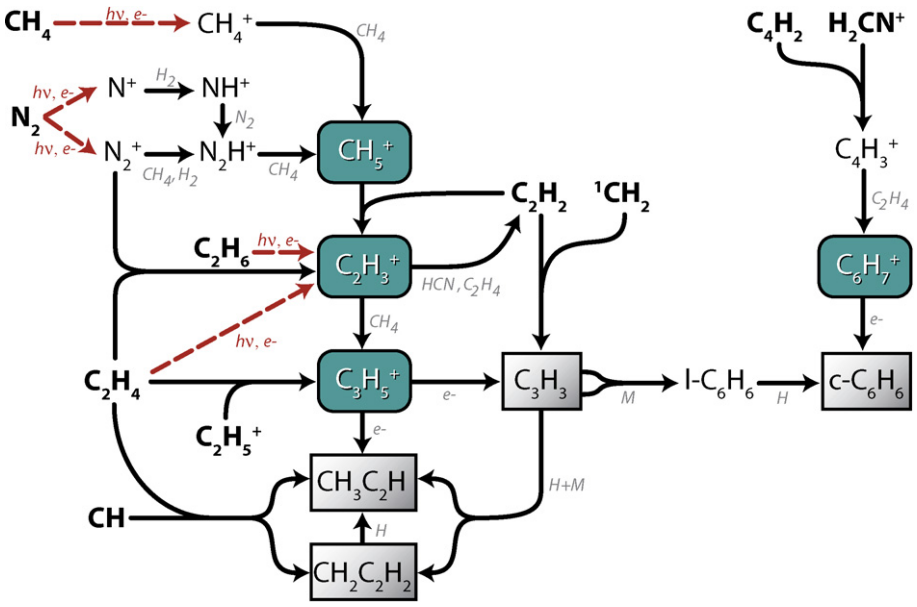

Fig. 12. Chemical scheme III. Coupled ion–neutral scheme leading to benzene and methylacetylene involving the formation of: CH_5^+, $C_2H_3^+$, $C_3H_5^+$, $C_4H_3^+$, $C_6H_7^+$, and C_3H_3. Species in bold are formed in previous chemical mechanisms.

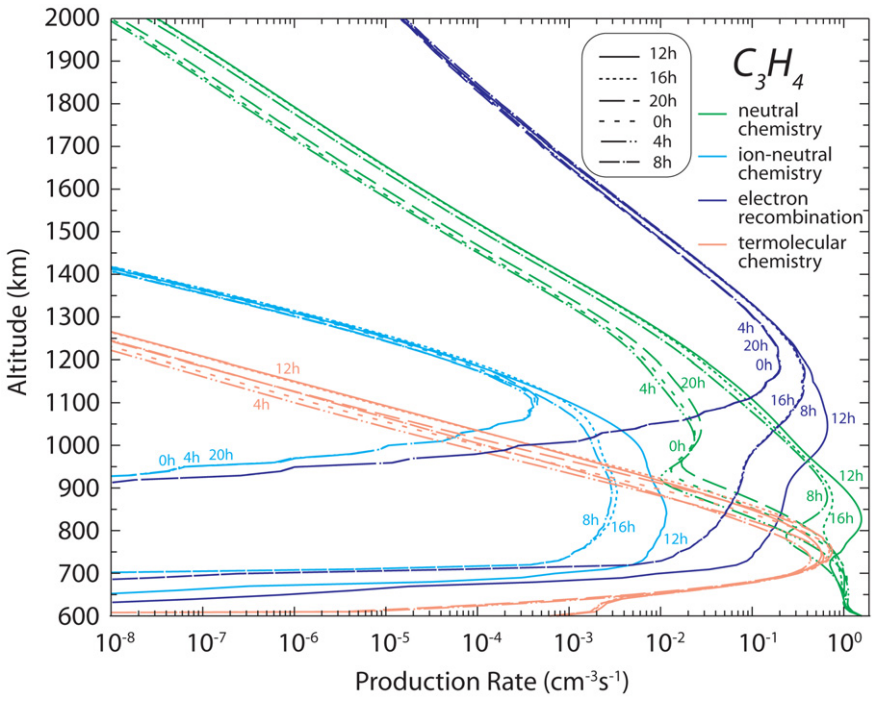

Fig. 13. Local time-dependent production rate profiles for CH_3C_2H, as computed by the present model for the T_A solar conditions, at a latitude of 38° North.

and ion–neutral mechanisms involving ions N^+, CNC^+ and HCN^+, and major hydrocarbons such as CH_4, C_2H_2 and C_2H_4.

4. Mixing ratio and density profiles

The local time-dependent density and mixing ratio neutral results are presented in Figs. 16–25 for the solar and latitudinal conditions of flybys T_A (blue) and T_5 (red). Four temporal snapshots were plotted corresponding to local times 12 h (overhead sun), 18 h, 0 h, and 6 h. The results are compared to those of Yung et al. (1984), Toublanc et al. (1995), Wilson and Atreya (2004), and Lebonnois (2005). Comparison is also provided with the N_2 and CH_4 INMS data recorded during T_A and T_5 (De La Haye et al., 2007a), the H_2 INMS T_A data (Yelle et al., 2006), the C_2H_2, C_2H_4, C_2H_6, C_3H_4, and Ar INMS data recorded at T_A's closest approach (Waite et al., 2005; Yelle et al., 2006), and the CH_4, C_2H_2, C_2H_4, and C_2H_6 UVIS T_A data (Shemansky et al., 2005). Numerical results are provided for these species in Table 2, and are compared to the models of Lebonnois (2005) and Wilson and Atreya (2004) at 600 and 1180 km and to the INMS data available at 1180 km. The local time-dependent density and mixing ratio profiles of HCN are also presented due to the key role of this species in the thermal structure of Titan's upper atmosphere.

For species N_2, CH_4, H_2, C_2H_4, C_2H_6, and Ar, the density profiles obtained are found to be nearly identical with respect to local time, suggesting stability and particularly long life times. For

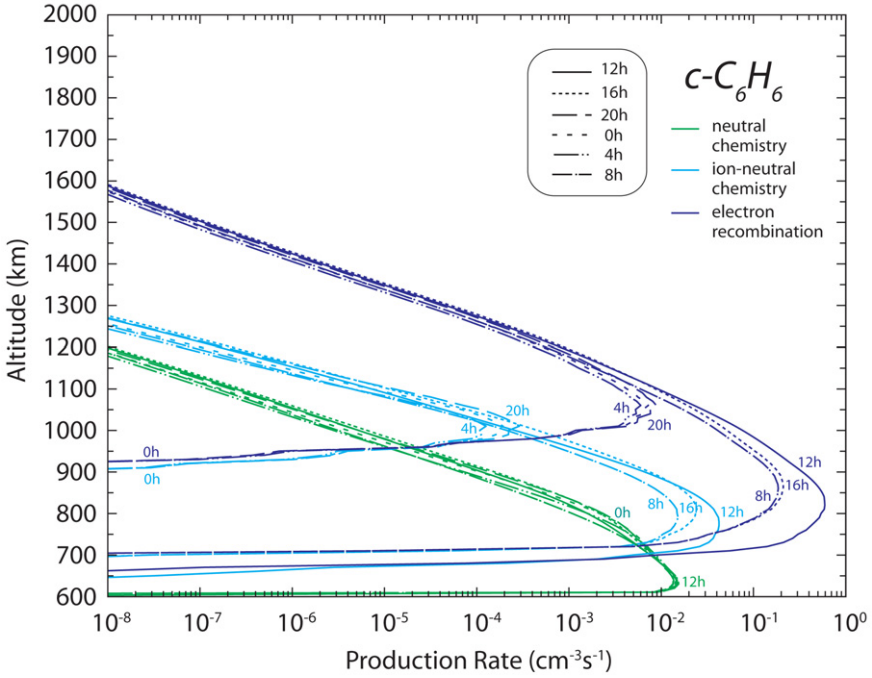

Fig. 14. Local time-dependent production rate profiles for c-C_6H_6, as computed by the present model for the T_A solar conditions, at a latitude of 38° North.

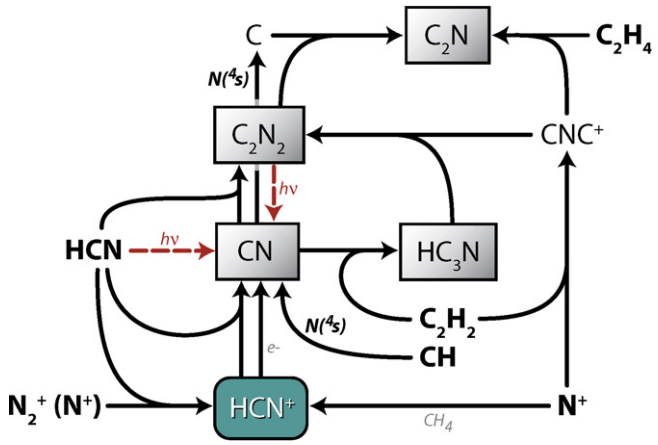

Fig. 15. Chemical scheme IV. Formation of the other nitrile compounds: CN, C_2N, C_2N_2, and HC_3N. Species in bold are formed in previous chemical mechanisms.

species C_2H_2, C_3H_4, and HCN, however, the local time profiles are distinct (Figs. 21, 23, and 24). These species have slightly shorter lifetimes due to a high dependence on solar driven mechanisms and on fast interactions with the ionosphere. For example, C_2H_2 results in large part from C_2H_4 photodissociation, and CH_3C_2H depends essentially on the amount of reactive species CH in the atmosphere (a product of C_2H_4 photodissocation) and on the electron recombination of $C_3H_5^+$ at higher altitudes. As for HCN, its local time-dependence is mainly due to fast neutral reactions initiated by the photodissociations of N_2 and CH_4 (see section on hydrogen cyanide).

4.1. Nitrogen and methane

The methane mixing ratios obtained at 1180 km in the present study (3.0–3.9%) are in good agreement with the INMS data (3.1–4.1%), and are factors 2 to 3 times smaller than the results of Lebonnois (2005) and Wilson and Atreya (2004). In addition, we find the CH_4 mixing ratio at 1180 km to be a factor of $2^{\pm 0.4}$ larger than at 600 km, compared to factors of 3.9 using the Lebonnois (2005) model and 4.3 using the model of Wilson and Atreya (2004). These differences in slope are induced by an eddy coefficient of 10^8 cm^2 s^{-1} above 900 km in Lebonnois (2005) compared to 4×10^9 cm^2 s^{-1} in the present model. The variations are accentuated when considering the Wilson and Atreya (2004) results (as well as the Yung et al., 1984 and Toublanc et al., 1995 results) due to differences in the input temperature profiles (Fig. 2).

After the analysis of the UVIS T_A data, Shemansky et al. (2005) reported CH_4 densities of 4.3×10^7 cm^{-3} at 1213 km, 8.3×10^7 cm^{-3} at 1350 km, and 1.3×10^7 cm^{-3} at 1397 km, larger than the T_A INMS data by factors of 2.3, 13.1, and 3.1, respectively. At 615 km, however, the UVIS value (1.6×10^{11} cm^{-3}) is 1.4 times smaller than that calculated by the present model, which matches the INMS data reasonably well at altitudes between 1174 and 1600 km (Fig. 17). Shemansky et al. (2005) also suggested a departure from a mixed to a diffusively separated atmosphere at ≃800 km, an altitude about 450 km lower than that derived after the atmospheric structure analysis of the T_A INMS data (De La Haye et al., 2007a). These discrepancies may be in part responsible for the differences in temperature profile between Shemansky et al. (2005) and the combined CIRS and INMS data.

The modeled N_2 and CH_4 density profiles are found to diverge from the INMS data (ingress and egress portions of T_A and egress portion of T_5) above 1700 km (Figs. 16 and 17). This divergence was studied in De La Haye et al. (2007a), suggesting significant heating mechanisms in Titan's upper atmosphere and the presence of a developed corona in the vicinity of Titan. The modeled N_2 and CH_4 mixing ratio profiles are also found to diverge from the data, but the trend starts at lower altitudes, i.e. 1500–1600 km, and is observed for all four datasets (ingress and egress portions of T_A and T_5). The mixing ratio-divergence is essentially due to H_2 becoming a major species at altitudes above 1500–1600 km, with a mixing ratio larger than 10%, and to a poor match of the modeled H_2 profiles with the INMS density data (see below).

4.2. Molecular hydrogen

For molecular hydrogen, the present model suggests mixing ratios between 4.1×10^{-3} and 5.6×10^{-3} at 1180 km, adequately

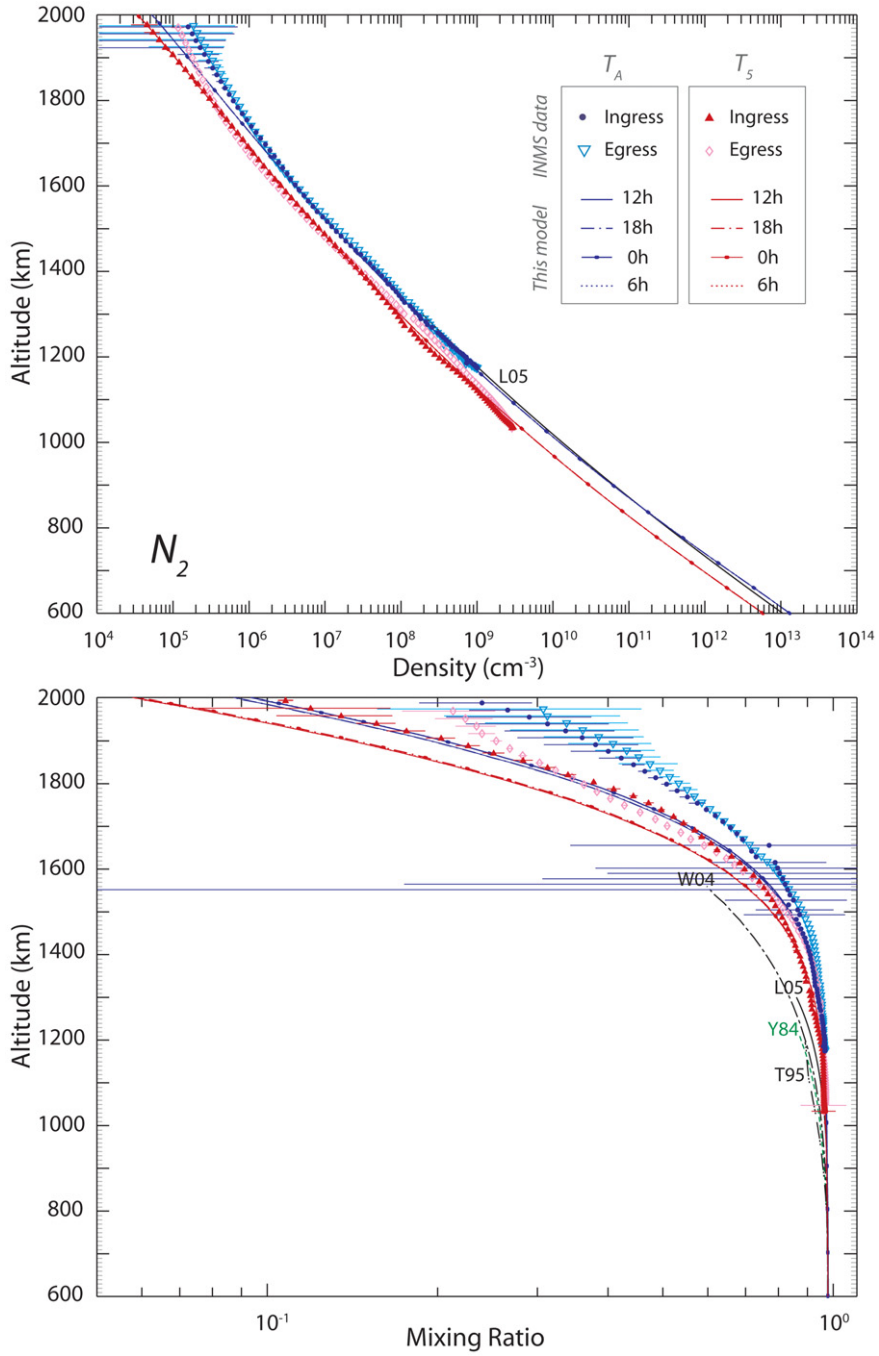

Fig. 16. Local time-dependent nitrogen profiles determined in the present work for the T_A and T_5 conditions at latitude 38.8° N and 71.6° N. L05 refers to results from the model developed in Lebonnois et al. (2001, 2003), and Lebonnois (2005), recently re-run at latitude 40° N and winter solstice, using the total density and temperature profiles of Vervack et al. (2004). The profiles of Yung et al. (1984), Y84, Toublanc et al. (1995), T95, Wilson and Atreya (2004), W04, are also displayed. These results are compared to the INMS density and mixing ratio data recorded during T_A and T_5 (De La Haye et al., 2007a). The error bars applied on the INMS density data do not take into account the systematic 20% instrumental uncertainty.

matching the T_A INMS data. However, as altitude increases, the model diverges from the data with higher densities than those estimated by measurement (Fig. 18), suggesting the need for an escape flux significantly larger than thermal escape to fit the INMS data.

A second run was performed for the T_A conditions, arbitrarily imposing an upper boundary of twice the Jeans escape (see pale blue lines in Fig. 18). This condition corresponds to a H_2 upward flux of 9.3×10^9 cm^{-2} s^{-1} referred to the surface, a value in good agreement with the value of $1.2 \pm 0.2 \times 10^{10}$ cm^{-2} s^{-1} calculated in Yelle et al. (2006). The second run is shown to provide a better fit of the INMS data at altitudes >1300 km, but leads to greater discrepancy at closest approach. The results suggest again the presence of non-thermal escape mechanisms, probably involving charge-exchange processes, sputtering, and ion pick-up. These mechanisms are not fully understood at the moment, and their inclusion is judged beyond the scope of the present study. The discrepancy between the modeled H_2 abundances and the data becomes important at altitudes above ≃1200 km, and is shown to have a negligible effect on the chemistry.

The H_2 mixing ratios of Lebonnois (2005) and Wilson and Atreya (2004) are 1.5 and 1.8 times smaller than the INMS mea-

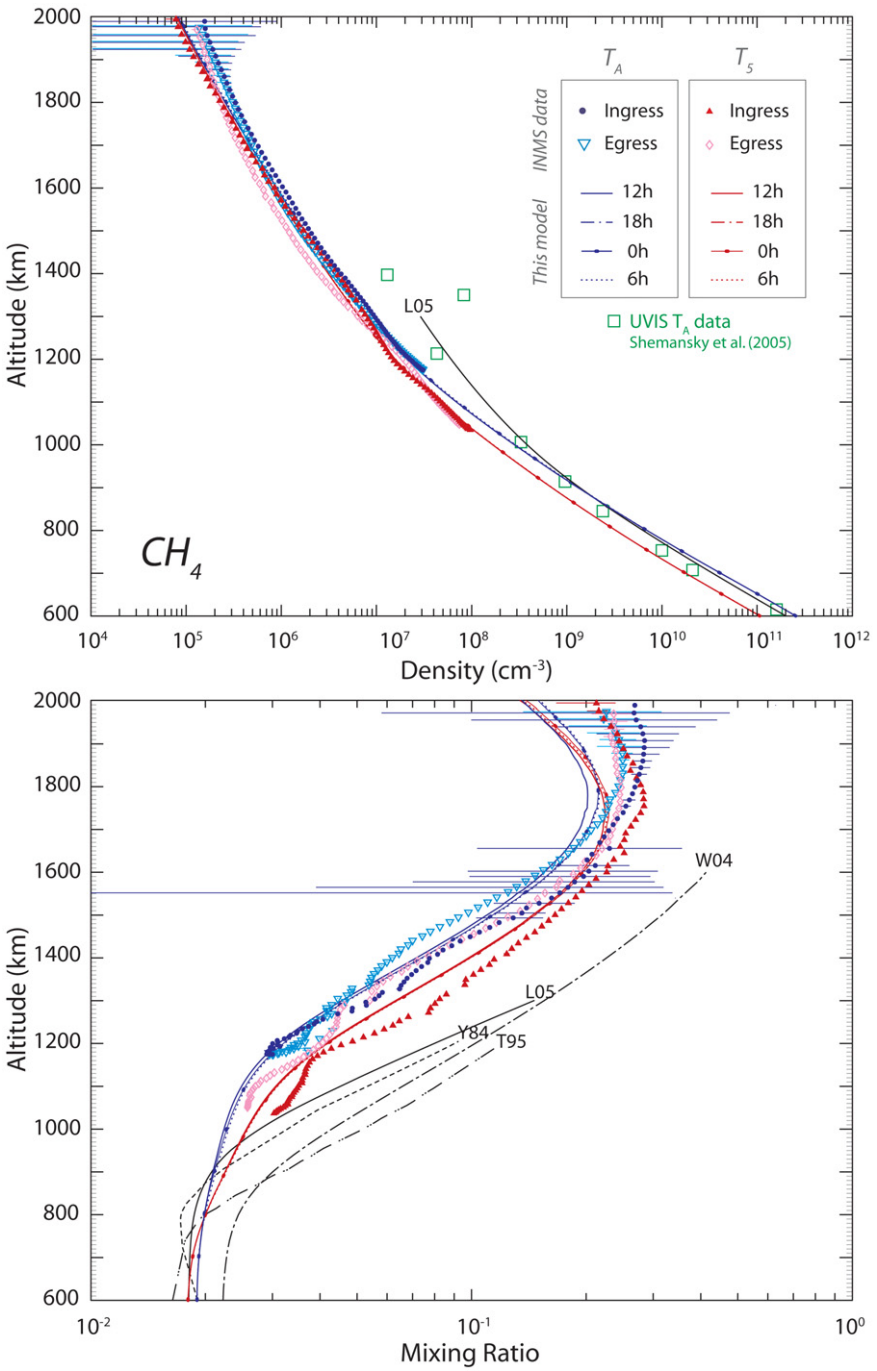

Fig. 17. Local time-dependent methane profiles determined in the present work for the T_A and T_5 conditions... (see legend of Fig. 16). These results are compared to the INMS density and mixing ratio data recorded during T_A and T_5 (De La Haye et al., 2007a).

surements at 1180 km, and 1.4 to 2.7 times smaller than the adjusted values used in the present model at 600 km (Table 2). These variations are due to the difference in the choice of the temperature and eddy coefficient profiles, and suggest a review of the H_2 production mechanisms below 600 km.

4.3. Ethylene

Large variations appear across models in the C_2H_4 mixing ratio profiles. In the lower panel of Fig. 19, two sets of local time-dependent results are presented, both corresponding to the T_A solar and latitudinal conditions. The first set of results, plotted in pale blue, used the C_2H_4 mixing ratio of Lebonnois (2005) as lower boundary condition. These profiles show large local-time variations corresponding to the dependence of C_2H_4 production on reactive species CH, $^3CH_2$, and CH_3, directly produced by methane photodissociation. Adequate match is found with the lowest of the two INMS data points proposed in Waite et al. (2005) for C_2H_4 at 1180 km. (The two INMS estimates, $2.6 \pm 0.7 \times 10^{-4}$ and $5.3 \pm 0.1 \times 10^{-4}$, depend on the value adopted for HCN in the mass spectral deconvolution of the T_A data.)

The differences observed between the present C_2H_4 results and those of Lebonnois (2005) suggest different production rates below 1000 km, therefore involving Eq. (1). Since the same reaction rates as Lebonnois (2005) were used for $CH + CH_4 \rightarrow C_2H_4 + H$ and $^3CH_2 + CH_3 \rightarrow C_2H_4 + H$, and since the methane density

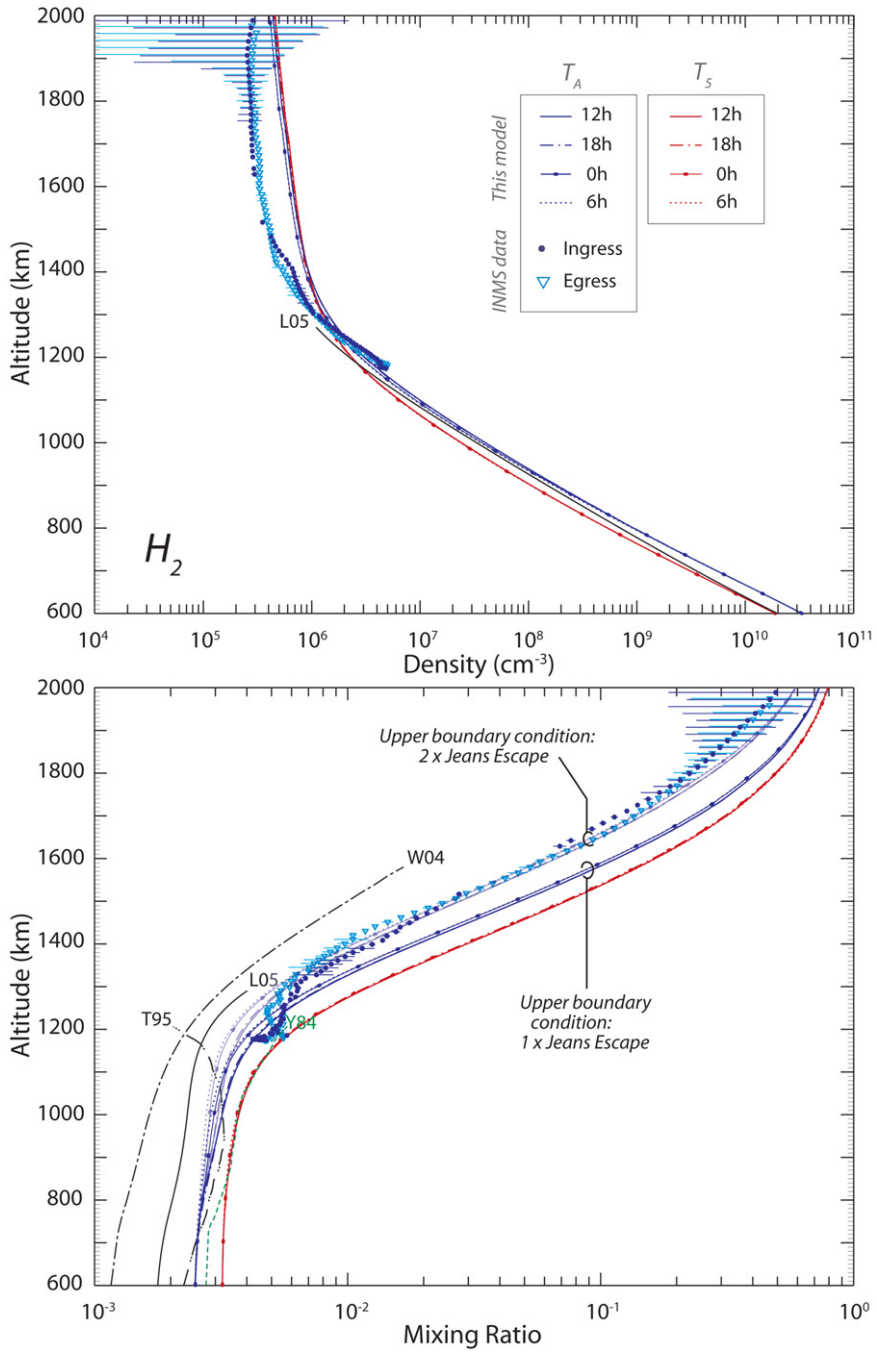

Fig. 18. Local time-dependent hydrogen profiles determined in the present work for the T_A and T_5 conditions… (see legend of Fig. 16). These results are compared to the INMS density and mixing ratio data recorded during T_A (Yelle et al., 2006). Two sets of local time-dependent results obtained with the present model are presented for the T_A conditions, one in dark blue using Jeans escape as upper boundary, and one in pale blue using twice the Jeans escape as upper boundary.

profiles are in good agreement below 1000 km (Fig. 17), the abundances of reactive species CH, $^3CH_2$, and CH_3 are examined. The local time-dependent density profiles of CH, $^3CH_2$, and CH_3 calculated in the T_A conditions are compared to Lebonnois (2005) in Fig. 20. Species CH and $^3CH_2$, which have short life times, are assumed to be in photochemical equilibrium at the lower boundary, and are found to nearly disappear at night. So due to the rotating method, the CH and $^3CH_2$'s densities are in average smaller than Lebonnois (2005) around 600 km. Contrary to CH and $^3CH_2$, which result almost solely from direct methane photodissociation, CH_3-production is also achieved on the night side through reactions $C_2H_5 + H \rightarrow CH_3 + CH_3$, $CH_4 + C_2 \rightarrow CH_3 + C_2H$, $CH_4 + C_2H \rightarrow CH_3 + C_2H_2$, and to a lesser extent $^1CH_2 + CH_4 \rightarrow CH_3 + CH_3$. For this reason, CH_3 has a longer lifetime, shows smaller local time variations, and does not disappear at night. In reaction $^3CH_2 + CH_3 \rightarrow C_2H_4 + H$ (integrated production rate of $\simeq 4 \times 10^7$ cm^{-2} s^{-1}), the effects of the lesser density of $^3CH_2$ compared to Lebonnois (2005) are compensated by the greater density of CH_3. However, in reaction $CH + CH_4 \rightarrow C_2H_4 + H$ (with an integrated production rate of $\simeq 2.5 \times 10^8$ cm^{-2} s^{-1}, about six times more efficient than the afore-mentioned process), the density of CH in average smaller than Lebonnois (2005) is directly responsible for the weaker C_2H_4-production at low altitudes. Sensitivity studies on the influence of the methane photodissociation scheme showed a maximum variation of the C_2H_4-production rate of less than 15% when comparing the scheme of Romani (1996) and those

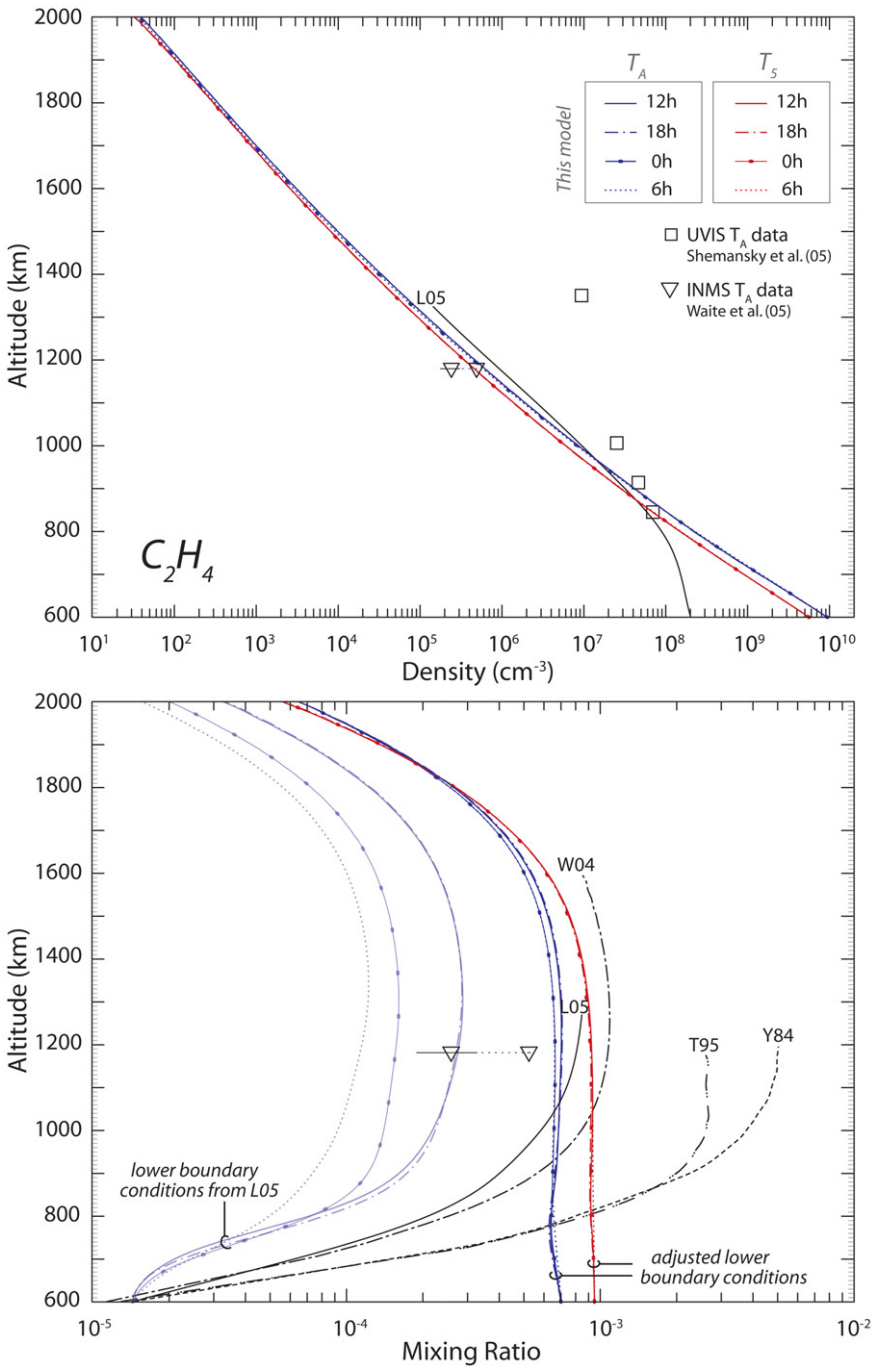

Fig. 19. Local time-dependent ethylene profiles determined in the present work for the T_A and T_5 conditions... (see legend of Fig. 16). These results are compared to the two T_A INMS data values suggested in Waite et al. (2005), depending on the value adopted for HCN. Two sets of local time-dependent results obtained with the present model are presented for the T_A conditions, one in pale blue using the Lebonnois (2005) mixing ratio at 600 km, and one in dark blue with adjusted lower boundary at 600 km. These latter results are the ones presented in Table 2.

of Mordaunt et al. (1993). These considerations suggest that the difference between the present results and those of previous models are mainly due to the local time-dependence of the model.

A second set of results, presented in dark blue, is provided to match the larger INMS value, in better agreement with predictions made by other models at high altitudes. In that case, the adjusted lower boundary mixing ratio is almost two orders of magnitude larger than that predicted by previous models at 600 km. With this large amount of ethylene at 600 km, the influence of chemical production becomes comparable to that of eddy and molecular diffusion, and the mixing ratio of C_2H_4 between 600 and 1300 km becomes quasi-constant. Such a high density of C_2H_4 at 600 km is improbable, and suggests the validity of the previous considerations.

The UVIS data available for species C_2H_4 are plotted in the upper panel of Fig. 19. Trends similar to the case of CH_4 are observed, with density slopes overall sharper in the UVIS data compared to the present model. The same observations will be apparent in the cases of C_2H_2 and C_2H_6 (Figs. 21 and 22): although the UVIS data between 600 and 800 km are found to be close to the values estimated with the present model, they are found to become significantly larger at $\simeq$1000 km.

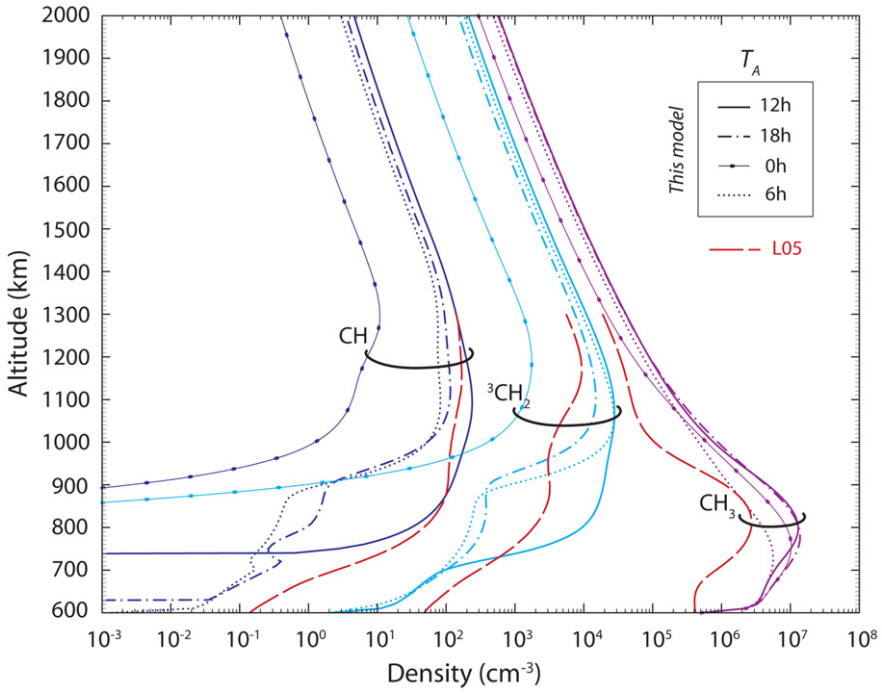

Fig. 20. Local time-dependent density profiles for CH, $^3CH_2$, and CH_3, computed using the present model in the T_A solar and latitudinal conditions, and taking into account both photo- and magnetospheric electrons. Comparison is provided with the Lebonnois (2005) results.

Table 2
Neutral results of the present model compared to the Lebonnois (2005) and Wilson and Atreya (2004) models at 1180 and 600 km

Latitude	Total density (cm^{-3})	Mixing ratios							
		N_2 ($\times10^{-2}$)	CH_4 ($\times10^{-2}$)	H_2 ($\times10^{-3}$)	C_2H_2 ($\times10^{-4}$)	C_2H_4 ($\times10^{-4}$)	C_2H_6 ($\times10^{-5}$)	C_3H_4[a] ($\times10^{-5}$)	Ar ($\times10^{-6}$)
1180 km									
Present work[b]									
38.8° (T_A)	8.8×10^8	96.4	3.0	4.1	2.2	6.8	9.4	0.90	8.0
73.7° (T_5)	4.9×10^8	95.4	3.9	5.6	2.4	9.2	10.3	0.53	6.2
Lebonnois (2005) model[c]									
40°	1.0×10^9	92.5	7.1	2.7	3.9	8.0	3.7	1.1	–
Wilson and Atreya (2004)[d]									
–	1.1×10^9	90.1	9.4	2.2	6.3	10.7	19.7	1.8	–
INMS data[e]									
38.8° (T_A)	$9.3^{\pm0.15} \times 10^8$	$96.4^{\pm0.02}$	$3.1^{\pm0.03}$	$4.05^{\pm0.03}$	$1.89^{\pm0.05}$	$5.3^{\pm0.1}$	$12.1^{\pm0.6}$	$0.386^{\pm0.022}$	$7.1^{\pm0.1}$
61.8° (T_5)	$6.1^{\pm0.01} \times 10^8$	$95.7^{\pm0.004}$	$3.8^{\pm0.001}$						
73.0° (T_5)	$4.4^{\pm0.02} \times 10^8$	$95.5^{\pm0.004}$	$4.1^{\pm0.008}$						
600 km									
Present work[b]									
38.8° (T_A)	1.3×10^{13}	97.8	1.9	2.5	0.5	7.0	10.0	0.01	11
73.7° (T_5)	5.9×10^{12}	97.8	1.8	3.2	1.25	9.5	11.5	0.5	11
Lebonnois (2005) model[c]									
40°	1.1×10^{13}	98.0	1.8	1.8	0.62	0.14	2.6	0.034	–
Wilson and Atreya (2004)[d]									
–	1.1×10^{13}	97.7	2.2	1.2	0.37	0.11	4.2	0.17	–

[a] Sum of the CH_3C_2H and $CH_2C_2H_2$ mixing ratios—CH_3C_2H only for the Wilson and Atreya (2004) results.
[b] Diurnal average results obtained using the solar conditions corresponding to flybys T_A (38.8° N) and T_5 (73.7° N). The mixing ratios at 600 km were adapted to match the INMS data at higher altitudes.
[c] Results from the model developed in Lebonnois et al. (2001, 2003) and Lebonnois (2005), recently re-run at latitude 40° N and winter solstice, using the total density and temperature of Vervack et al. (2004).
[d] Results of Wilson and Atreya (2004) obtained with a 58° zenith angle for a globally averaged solar flux in Nov. 1980.
[e] INMS data recorded during T_A (38.8° N) for H_2, C_2H_2, C_2H_4, C_2H_6, C_3H_4 and Ar (Waite et al., 2005) and during T_A (38.8° N) and T_5 (61.8° N and 73.0° N) for N_2 and CH_4 (De La Haye et al., 2007a).

4.4. Acetylene, ethane, methylacetylene

The local time variations that were noted in the C_2H_2 production rates (Fig. 10) also appear in the modeled density profiles (Fig. 21). These profiles agree reasonably well with the results of Lebonnois (2005) and Wilson and Atreya (2004). The mixing ratio slopes between 600 and 800 km are found to be in average sharper in the T_A (blue) compared to the T_5 (red) conditions. This differ-

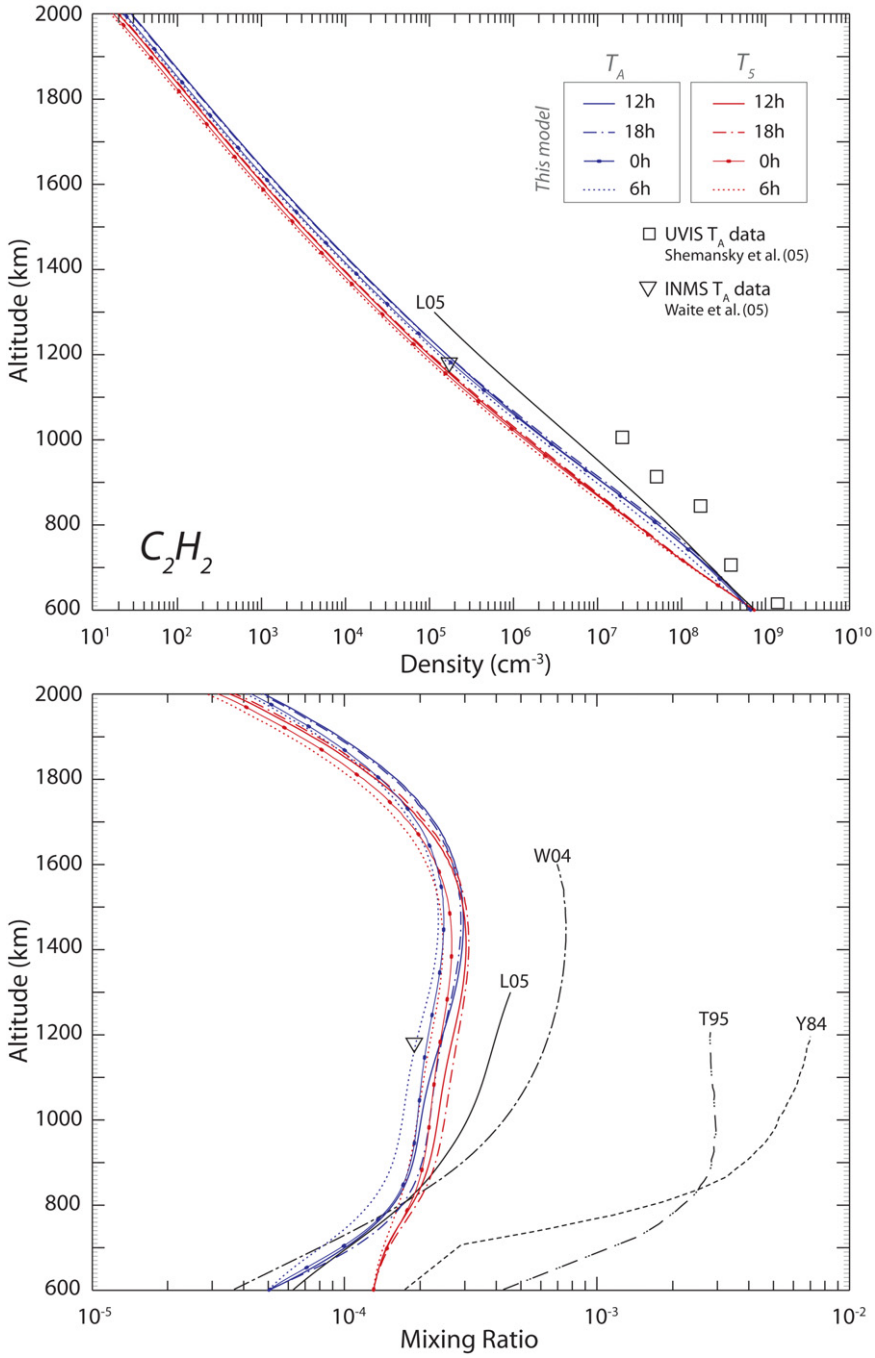

Fig. 21. Local time-dependent acetylene profiles determined in the present work for the T_A and T_5 conditions... (see legend of Fig. 16). These results are compared to the INMS density and mixing ratio data recorded during T_A (Waite et al., 2005).

ence is due to a more efficient production of acetylene through ethylene photodissociation between 600 and 800 km during the T_A rotation (zenith angle at noon of 61°) compared to the T_5 rotation (zenith angle at noon of 90°). Due to differences in eddy coefficient and temperature and to adjustment in mixing ratio at the lower boundary, the results of the present model at 1180 km are found to be in better agreement than Lebonnois (2005) and Wilson and Atreya (2004) with the C_2H_2 and C_2H_6 INMS data (Table 2). Larger discrepancies are observed with the results of Yung et al. (1984) and Toublanc et al. (1995), as shown in Figs. 21 and 22.

For minor species C_2H_6, the results of the various models disagree in the altitude region between 600 and 900 km: the present model shows mixing ratios that remain quasi-constant, whereas the Lebonnois (2005) and Wilson and Atreya (2004) models suggest mixing ratios increasing rapidly with altitude. In this altitude range, the ethane production rate is dominated by $CH_3 + CH_3 \xrightarrow{M} C_2H_6$, and the difference is likely due to the large uncertainties associated with the methyl recombination rate (Vuitton and Yelle, 2005; Wilson and Atreya, 2004). The rates of Slagle et al. (1988) were adopted in the present model ($k_0 = 8.76 \times 10^{-6} \times T^{-7.03} e^{-\frac{1390}{T}}$, $k_{\inf} = 1.5 \times 10^{-6} \times T^{-1.18} e^{-\frac{329}{T}}$), in good agreement with the experiments of Cody et al. (2003) conducted at 155 K (He-background gas). Wilson and Atreya (2004) estimated these rates to be about an order of magnitude too low for a N_2-background gas, and chose to use the Slagle et al. (1988)

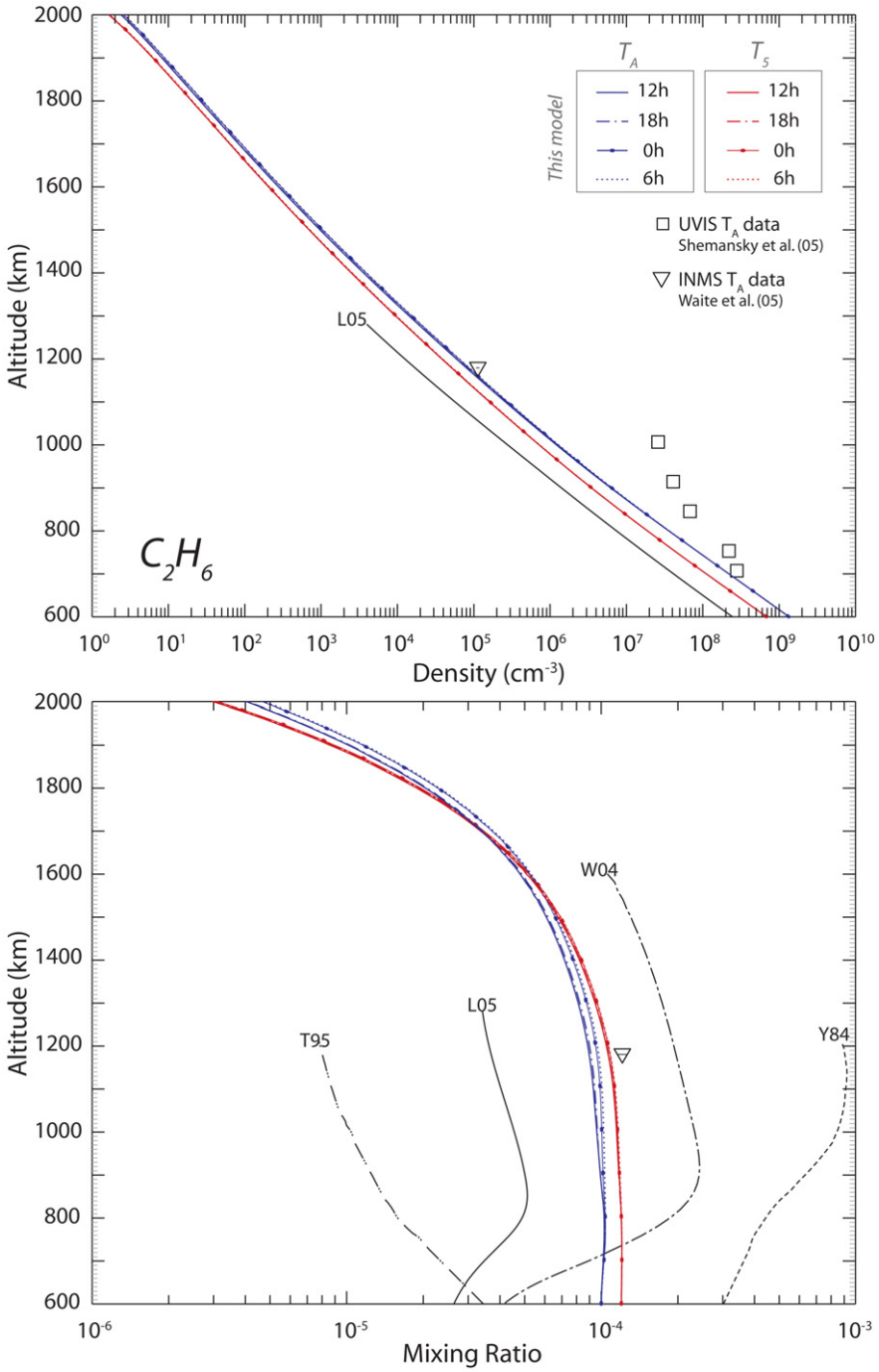

Fig. 22. Local time-dependent ethane profiles determined in the present work for the T_A and T_5 conditions... (see legend of Fig. 16). These results are compared to the INMS density and mixing ratio data recorded during T_A (Waite et al., 2005).

expression but multiplied by 10. In the Lebonnois (2005) model, another expression was used, based on Lee et al. (2000), $k_0 = 6 \times 10^{-29} \times e^{\frac{1680}{T}}$, and Du et al. (1996), $k_{\text{inf}} = 1.53 \times 10^{-7} \times T^{-1.2} e^{-\frac{295}{T}}$. So, assuming a total density of 1.1×10^{13} cm^{-3} and a temperature of $\simeq$150 K, the methyl recombination rate used in the present model is about five times lower than Lebonnois (2005), and ten times lower than Wilson and Atreya (2004). Sensitivity studies show that such a difference in reaction rate justifies the variations between the modeled C_2H_6 below 900 km. These considerations lead to the following hypotheses: (1) the methyl recombination rate is an order of magnitude larger than that determined by Slagle et al. (1988) and Cody et al. (2003), in which case further experimental studies on that reaction need to be made in the adequate temperature and pressure conditions, or (2) the C_2H_6 mixing ratio at 600 km is 4 to 8 times larger than the mixing ratios 4.2×10^{-5} and 2.6×10^{-5} proposed by the Wilson and Atreya (2004) and Lebonnois (2005) models, respectively, implying the presence of additional sources of ethane below 600 km. However, it is not clear at this point what mechanism other than Eq. (10) could have such an influence at low altitudes on the ethane production rate, and this alternative may also call for the consideration of the first hypothesis. The local time-dependent abundance of radical CH_3 is another factor to consider in the study of C_2H_6 production. Sensitivity studies on the methane photodissociation schemes showed a maximum variation of $\simeq$18% when using the first scheme of Mordaunt et al. (1993), with a CH_3-quantum yield

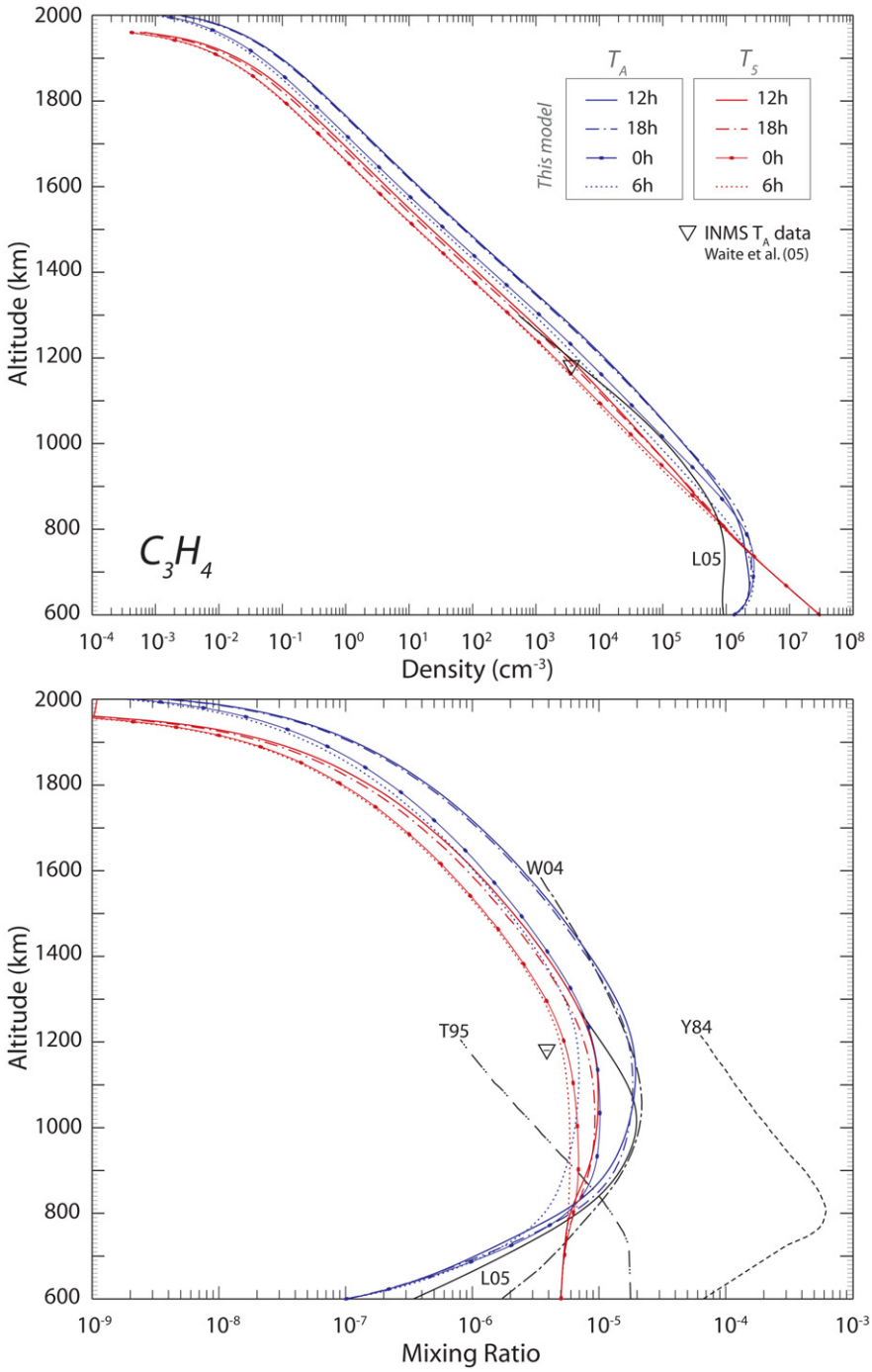

Fig. 23. Local time-dependent C_3H_4 profiles determined in the present work for the T_A and T_5 conditions... (see legend of Fig. 16). These results are compared to the INMS density and mixing ratio data recorded during T_A (Waite et al., 2005).

of 0.51, compared to that of Romani (1996), with a CH_3-quantum yield of 0.41. This variation, although non-negligible, is insufficient for explaining the afore-mentioned difference in the C_2H_6 production.

The local time-dependent density profiles of C_3H_4, obtained by adding the densities of CH_3C_2H and its less abundant isomer $CH_2C_2H_2$, are shown in Fig. 23 for the T_A and T_5 conditions. As was the case for acetylene, a difference of slope is observed between the modeled T_A or T_5 C_3H_4-mixing ratio profiles between 600 and 900 km, suggesting a production rate significantly greater in the T_A conditions compared to the T_5 conditions. This difference is due, in particular, to the effect of reaction $C_3H_3 + H \xrightarrow{M} C_3H_4$ [Eq. (14)]. The rate of this termolecular reaction increases with increasing total density, $k = k_0 k_\infty n/(k_0 n + k_\infty)$, and is therefore more efficient at producing C_3H_4 during the simulation reproducing the T_A conditions, where the total density is greater by a factor of 2 compared to T_5.

4.5. Hydrogen cyanide

Important horizontal variations are obtained in the modeled HCN density and mixing ratio profiles (Fig. 24). They are induced by reaction $H_2CN + H \rightarrow HCN + H_2$, the main production mechanism of HCN between 600 and 900 km. These local time variations

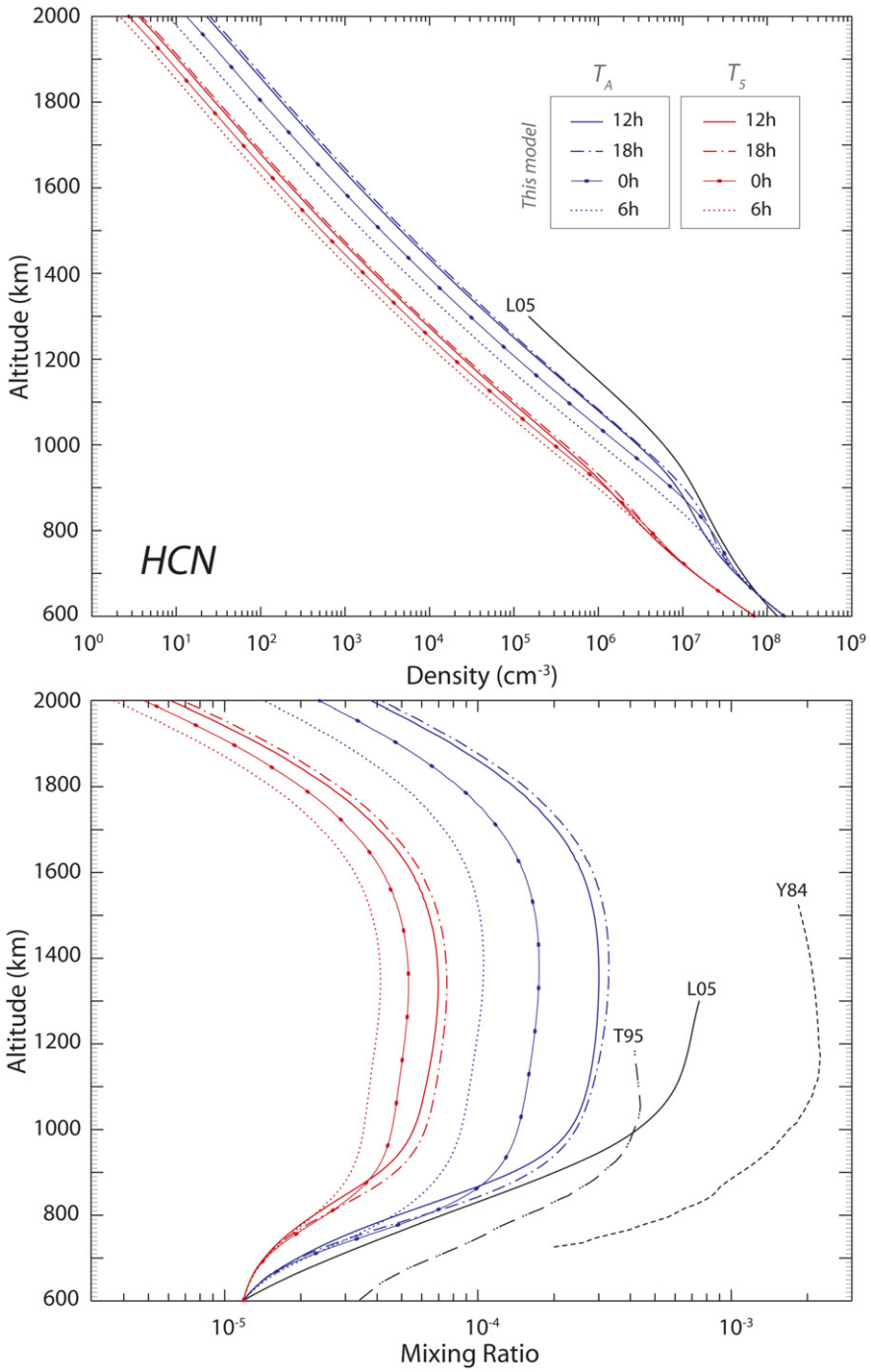

Fig. 24. Local time-dependent HCN profiles determined in the present work for the T_A and T_5 conditions... (see legend of Fig. 16).

are due to reactive species H_2CN resulting essentially from the reaction of $N(^4S)$ with CH_3, themselves produced by photodissociation of N_2 and CH_4. As a result, a significant depletion of H_2CN is found on the night side, with an order of magnitude of difference between noon and midnight: the H_2CN mixing ratio during the T_A simulation was found to be 2.1×10^{-5} at zenith angle 62° and 2.5×10^{-6} at zenith angle 165°.

Due to its main production mechanism being significantly reduced on the night side, the concentration of HCN obtained with the present rotating method is found to be lower overall than previous 1D-models. We find diurnally-averaged HCN mixing ratios of 1.2×10^{-5} at 600 km (lower boundary fixed using the Lebonnois, 2005 model), increasing to 2.2×10^{-4} (T_A) and 5.8×10^{-5} (T_5) at 1200 km, compared to $\simeq 4 \times 10^{-5}$ at 600 km and $\simeq 5 \times 10^{-4}$ at 1200 km calculated by Toublanc et al. (1995). In addition, the value suggested by Vuitton et al. (2006b) from the T_5 ionospheric observations (2×10^{-4} at 1100 km) is in good agreement with the present T_A-results, but is about 3 to 4 times larger than the present T_5-results.

To provide an indication of the minor density profiles, and to allow for relative comparison between species, diurnally averaged profiles are displayed in Fig. 25 for all the modeled neutrals. These profiles were determined by adding the density profiles obtained

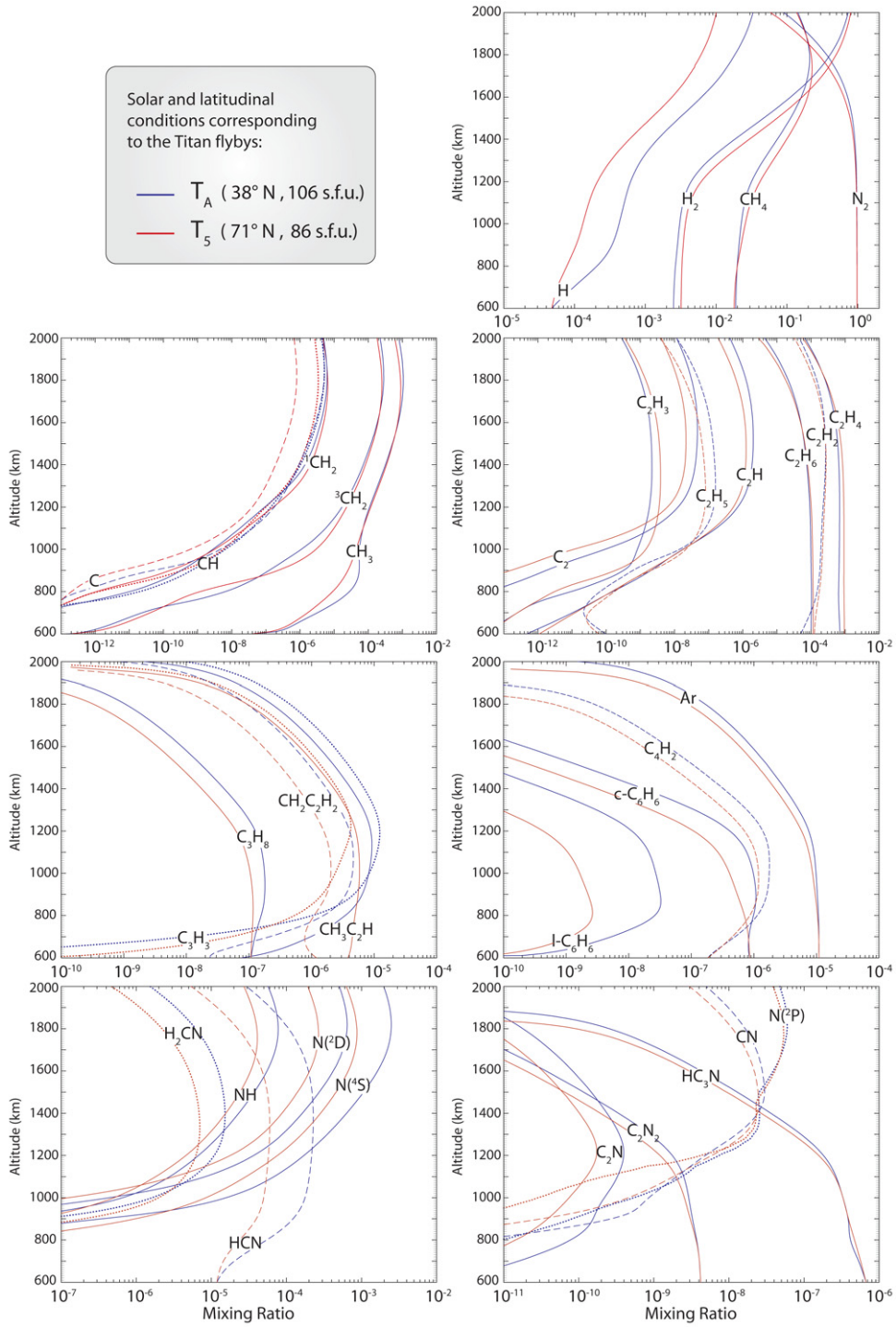

Fig. 25. Neutral mixing ratio profiles obtained using the present coupled ion–neutral rotating model in the T_A and T_5 solar and latitudinal conditions, diurnally averaged at latitude 38.8° N and 71.6° N, respectively, and taking into account both photo- and magnetospheric electrons.

at the center-time of each local time sector and dividing by the number of sectors.

4.6. Ionosphere

Prior to the first in situ ion composition measurements made by the Cassini INMS (Cravens et al., 2006), ionospheric models (e.g. Fox and Yelle, 1997; Keller et al., 1998; and Banaszkiewicz et al., 2000) included most of the key hydrocarbon ion species (CH_5^+, $C_2H_5^+$, $C_3H_5^+$, ...) and some of the key nitrile ion species (H_2CN^+, C_3HN^+, ...). The T_5 INMS measurements, however, revealed several interesting omissions in these models' ion–neutral chemical schemes. For example, the measured ion mass spectra had significant mass 18 and 30 peaks (Cravens et al., 2006) that were not predicted by the models. In order to remedy this situation, Vuitton et al. (2006b) expanded the ion–neutral chemical scheme by including a number of new nitrile species, both ionized and neutral. The $m = 18$ species was attributed to NH_4^+ which is produced by the reaction of any major ion species with ammonia (NH_3). The $m = 30$ species was identified as $CH_2NH_2^+$ which comes from reaction of major species (such as H_2CN^+) with CH_2NH. Other ion species considered by Vuitton et al. (2006b) include $C_2H_3CNH^+$

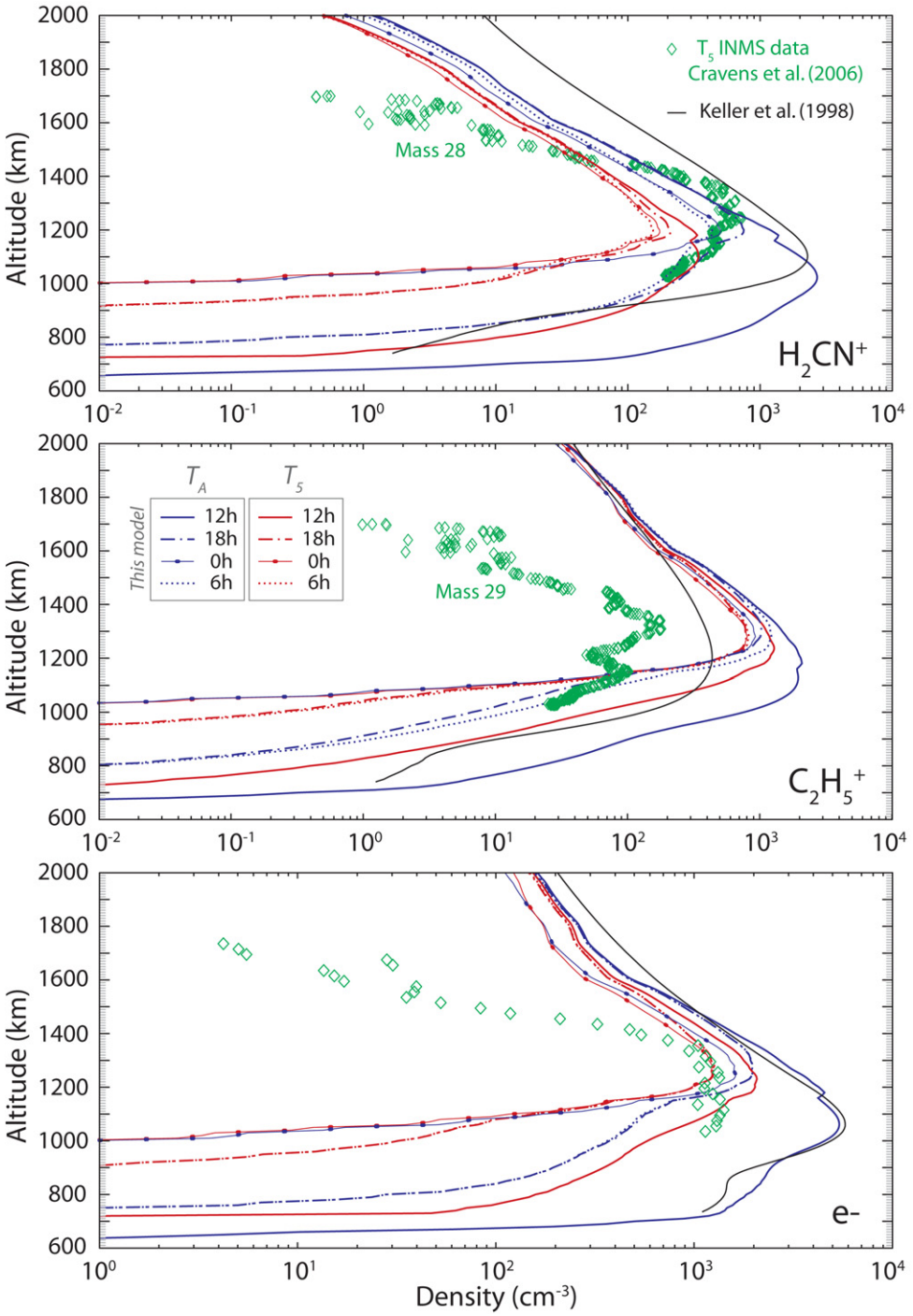

Fig. 26. Local time-dependent H_2CN^+, $C_2H_5^+$, and thermal electron density profiles determined in the present work for the T_A and T_5 conditions, taking into account both photo- and magnetospheric electrons. The results are compared to the model of Keller et al. (1998) and to the INMS ion data recorded during T_5 (Cravens et al., 2006).

($m = 54$) and $C_4H_3NH^+$ ($m = 66$). The additional nitrile species and ion–neutral chemistry discussed by Vuitton et al. (2006b) become important quantitatively at altitudes <1100 km, with a contribution of ≃15% to the total ion density at 1100 km.

Further work is required on the ionospheric modeling component of the present model (based on the chemical scheme of Keller et al., 1998), especially to include these additional ions. This work is deemed outside of the scope of the present study, largely because the neutral mode of Cassini INMS is not sensitive enough to detect the quantities of the required minor neutral species (e.g. NH_3 or CH_2NH). Furthermore, the understanding of the interaction between Titan and Saturn's magnetosphere remains limited, making difficult the quantitative modeling of night side ionization source, presumably due to magnetospheric electrons. Nonetheless, the chemical scheme of Keller et al. (1998) handles the most abundant ion species reasonably well at altitudes >1100 km (in particular, $C_2H_5^+$ and H_2CN^+), and the present study brings an important contribution to the understanding of Titan's upper atmosphere, in that it couples the neutral and ion chemistry and includes local time-dependence in the ionization sources and neutral atmosphere.

The local time-dependent density profiles are presented for the major ions H_2CN^+ and $C_2H_5^+$ and for the thermal electrons in Fig. 26. The Keller et al. (1998) results computed in the Voyager

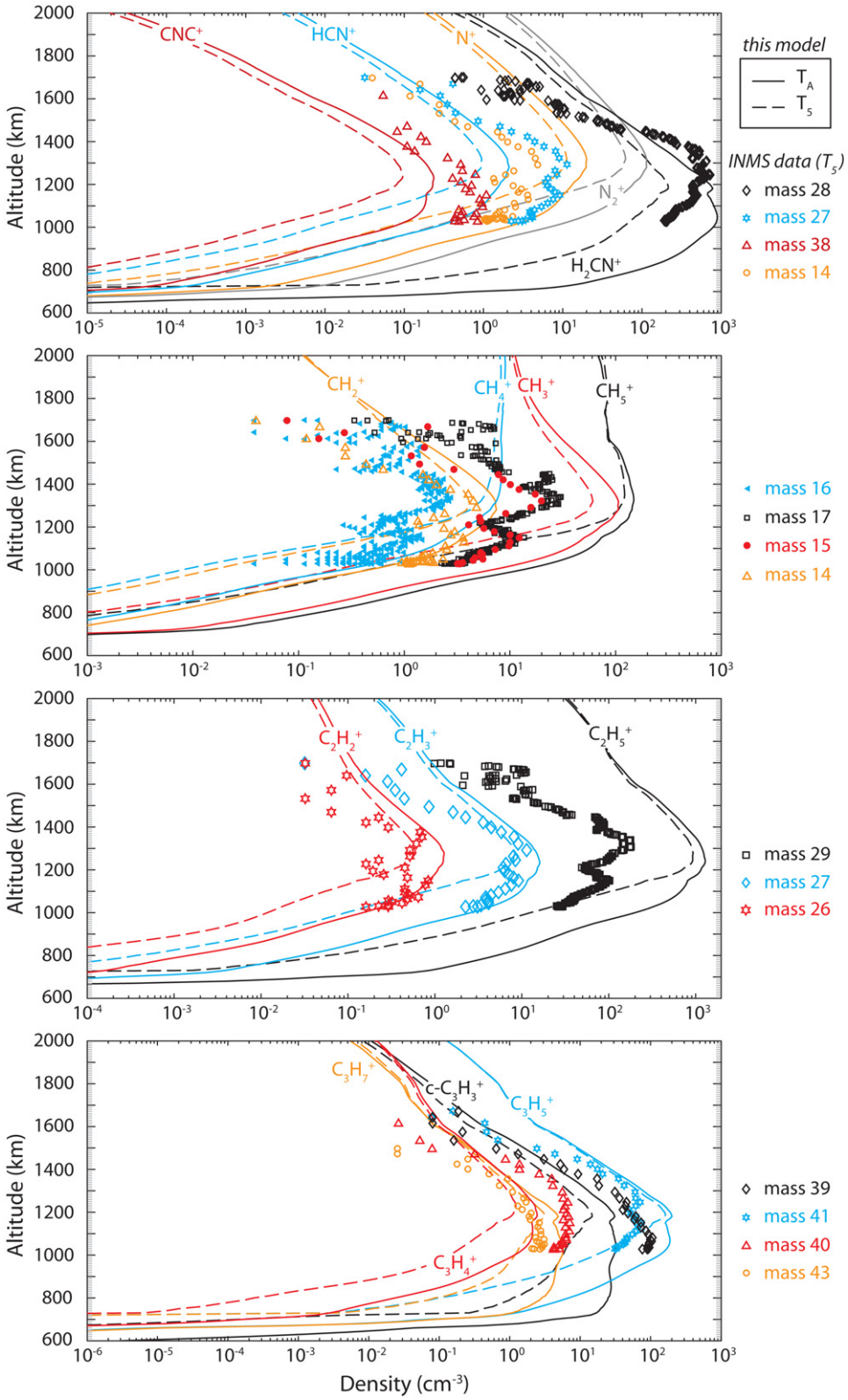

Fig. 27. Diurnally-averaged ion density profiles determined in the present work for the T_A and T_5 conditions, taking into account both photo- and magnetospheric electrons. The results are compared to the INMS ion data recorded during T_5 (Cravens et al., 2006).

solar conditions at a zenith angle of 60°, using the neutral model of Yung et al. (1984) as background, are also plotted and compared to the INMS ionospheric data reported in Cravens et al. (2006).

Larger local time variations are observed in the T_A compared to the T_5 configuration, since the rotation encompasses a wider range of zenith angles. For T_A, the electron peak varies between 5.4×10^3 cm^{-3} at 1060 km (noon) and 1.6×10^3 cm^{-3} at 1250 km (midnight). For T_5, the electron peak remains in the same altitude region (1230 to 1280 km), with values varying between 2.1×10^3 cm^{-3} (noon) and 1.3×10^3 cm^{-3} (midnight). These re-

sults are in reasonable agreement with Keller et al. (1992), who reported peak electron densities of 6.2×10^3 cm^{-3} at 1055 km and 3.03×10^3 cm^{-3} at 1175 km for zenith angles of 60° and 90°, respectively. The electron peak measured by INMS during T_5, $>10^3$ cm^{-3}, was found to be at $\simeq$1120 km (Cravens et al., 2006), about 100 km lower than suggested by the present model.

The modeled densities for H_2CN^+, the most abundant ion species, are found to agree reasonably well with the T_5 density data (i.e., within a factor of 2), indicating a reasonable overall ionization rate for the nightside. However, although the modeled $C_2H_5^+$ densities are in good agreement for altitudes below about 1100 km, the densities near 1300 km are about a factor of 5 higher than the measured densities. If the modeled abundance of neutral HCN was higher by a factor of 2–3 near 1200 km, the $C_2H_5^+$ density would be lower and the H_2CN^+ density would be higher, thus improving the data–model comparisons for both species. [Recall that the major source of H_2CN^+ is through reaction $C_2H_5^+ + HCN \rightarrow H_2CN^+ + C_2H_4$, Eq. (3)]. However, such arbitrary fixes are not possible in a self-consistent coupled ion–neutral model.

A selection of diurnally-averaged ion density profiles are displayed in Fig. 27, corresponding to results obtained by the present model for the T_A and T_5 solar and latitudinal conditions. The available INMS ionospheric data were also plotted for comparison (Cravens et al., 2006). The T_5 model–data comparison for masses 15 (CH_3^+) and 16 (CH_4^+) are reasonably good (factors of 2 to 3). CH_3^+ is produced by the reaction of N_2^+ with methane, and CH_4^+ is a "primary" ion species. This agreement indicates that the overall ionization rate used for the night side (electron impact) is about right. The modeled density of CH_5^+ (mass 17) agrees reasonably well with the data at 1100 km, but is about 5 times too high at 1200 km. CH_5^+ is produced by the reaction of CH_4^+ with methane and is lost by reacting with C_2H_2, C_2H_4, and H_2. Better agreement would be obtained if lower densities were found for any of these neutral species. The T_5 model–data comparisons for $C_2H_2^+$, $C_2H_3^+$, $C_3H_5^+$, $C_3H_3^+$, $C_3H_4^+$, and $C_3H_7^+$ are reasonable.

5. Conclusions

A one-dimensional coupled ion and neutral model was constructed to describe Titan's upper atmosphere, taking into account solar and magnetospheric energy inputs, and using updated temperature and eddy coefficient parameters. After consideration of the various processes' time scales, a rotating method was proposed to take into account the changes in solar radiation encountered by atmospheric particles.

The study of the comparative influences of photodissociation, neutral–neutral chemistry, ion–neutral chemistry, and electron recombination on the production rates of key neutral species was provided with respect to altitude and local time. The model showed large variations in the processes prevalent on the day compared to the night side, and evidenced the importance of ion–neutral chemistry and electron recombination on the neutral production rates at high altitude ($z > 1000$–1200 km). Considering the low atmospheric density at high altitude, these processes were found to have a limited impact on the overall density profiles of neutrals with long life-times. Their density profiles, contrary to species with short lifetimes (neutral radicals and ions), showed little local time-variation.

The observation of waves in Titan's upper atmosphere (Müller-Wodarg et al., 2006) underscored the significance of vertical and horizontal dynamics and the limits of one-dimensional models for describing Titan's neutral and ion composition. The understanding of Titan's upper atmosphere may require the construction of a new generation of three-dimensional dynamic models, taking into account the effects of ion–neutral chemistry, atmospheric waves, and the deposition of highly energetic particles from Saturn's magnetosphere. The present study proposes for that matter a simplification to an independent 19-species chemical scheme, starting with the photo- and electron impact ionization and dissociation of N_2, CH_4, and involving the strong coupling of key neutrals (C_2H_4 and HCN) and ions (H_2CN^+, $C_2H_5^+$, and CH_3^+) in Titan's upper atmosphere.

Ion and neutral exothermic chemistry represents an important source of heat in Titan's upper atmosphere. The present model is used in subsequent studies as basis for describing Titan's local time-dependent heating mechanisms and efficiencies.

Acknowledgments

This research was supported by the NASA Jet and Propulsion Laboratory contract 1283095, NASA task order NMO710023, *Support INMS Instrument on Cassini Spacecraft During Tour*. The authors thank R.V. Yelle and V. Vuitton of the University of Arizona for their input on the neutral model.

References

Andrieux, D., Bénilan, Y., de Vanssay, E., Paillous, P., Khlifi, M., Raulin, F., Bruston, P., Guillemin, J.-C., 1995. Absorption coefficient of propynenitrile in the mid-UV range for the study of Titan's atmosphere: Solution to sample constraints. J. Geophys. Res. 100, 9455–9460.

Anicich, V.G., 2003. An index of the literature for bimolecular gas phase cation-molecule reaction kinetics. Publication 03-19, JPL.

Au, J.W., Cooper, G., Burton, G., Olney, T.N., Brion, C.E., 1993. The valence shell photoabsorption of the linear alkanes, C_nH_{2n+2} ($n = 1$–8), absolute oscillator strengths (7–220 eV). J. Chem. Phys. 173, 209–239.

Backx, C., Wight, G.R., der Wiel, M.J.V., 1976. Oscillator strengths (10–70 eV) for absorption, ionization and dissociation in H_2, HD and D_2, obtained by an electron–ion coincident method. J. Phys. B 9, 315–331.

Banaszkiewicz, M., Lara, L.M., Rodrigo, R., López-Moreno, J.J., Molina-Cuberos, G.J., 2000. The upper atmosphere and ionosphere of Titan: A coupled model. Adv. Space Res. 26, 1547–1550.

Banks, P.M., Kockarts, G., 1973. Aeronomy. Academic Press, New York.

Bénilan, Y., Bruston, P., Raulin, F., Cossart-Magos, C., Guillemin, J.-C., 1994. Mid-UV spectroscopy of propynenitrile at low temperature: Consequences on expected results from observations of Titan's atmosphere. J. Geophys. Res. 99, 17069–17074.

Brook, E., Harrison, M.F.A., Smith, A.C.H., 1978. Measurements of the electron impact ionization cross sections of He, C, O and N atoms. J. Phys. B 11, 3115–3132.

Bruston, P., Poncet, H., Raulin, F., Cossart-Magos, C., Courtin, R., 1989. UV spectroscopy of Titan's atmosphere, planetary organic chemistry, and prebiological synthesis. Icarus 78, 38–53.

Chang, A.H.H., Mebel, A.M., Yang, X.M., Lin, S.H., Lee, Y.T., 1998. Ab initio/RRKM approach toward the understanding of ethylene photodissociation. J. Chem. Phys. 109, 2748–2761.

Chen, F.Z., Wu, C.Y.R., 2004. Temperature-dependent photoabsorption cross sections in the VUV–UV region. I. Methane and ethane. J. Quant. Spectrosc. Radiat. Trans. 85, 195–209.

Clarke, D.W., Ferris, J.P., 1995. Photodissociation of cyanoacetylene: Application to the atmospheric chemistry of Titan. Icarus 115, 119–125.

Clarke, D.W., Ferris, J.P., 1996. Mechanism of cyanoacetylene photochemistry at 185 nm and 254 nm. J. Geophys. Res. 101, 7575–7584.

Cody, R.J., Romani, P.N., Nesbitt, F.L., Iannone, M.A., Tardy, D.C., Stief, L.J., 2003. Rate constant for the reaction $CH_3 + CH_3 \rightarrow C_2H_6$ at $T = 155$ K and model calculation of the CH_3 abundance in the atmospheres of Saturn and Neptune. J. Geophys. Res. 108, doi:10.1029/2002JE002037.

Connors, R.E., Roeber, J.L., Weiss, K., 1974. Vacuum ultraviolet spectroscopy of cyanogen and cyanoacetylenes. J. Chem. Phys. 60, 5011–5024.

Cooper, G., Burton, G.R., Brion, C.E., 1995. Absolute UV and soft X-ray photoabsorption of acetylene by high resolution dipole (e, e) spectroscopy. J. Electron. Spectrosc. 73, 139–148.

Cravens, T.E., Robertson, I.P., Waite Jr., J.H., Yelle, R.V., Kasprzak, W.T., Keller, C.N., Ledvina, S.A., Niemann, H.B., Luhmann, J.G., McNutt, R.L., Ip, W.-H., De La Haye, V., Müller-Wodarg, I., Wahlund, J.-E., Anicich, V.A., Vuitton, V., 2006. The composition of Titan's ionosphere. Geophys. Res. Lett. 33. L07,105.

De La Haye, V., 2005. Coronal formation and heating efficiencies in Titan's upper atmosphere: Construction of a coupled ion neutral and thermal structure model to interpret the first INMS Cassini data. Ph.D. thesis, University of Michigan.

De La Haye, V., Waite Jr., J.H., Johnson, R.E., Yelle, R.V., Cravens, T.E., Luhmann, J.G., Kasprzak, W.T., Gell, D.A., Magee, B., Leblanc, F., Michael, M., Jurac, S., Robertson, I.P., 2007a. Cassini ion and neutral mass spectrometer data in Titan's upper atmosphere and exosphere: Observation of a suprathermal corona. J. Geophys. Res. 112, doi:10.1029/2006JA012222. A07,309.

De La Haye, V., Waite Jr., J.H., Cravens, T.E., Nagy, A.F., Yelle, R.V., Johnson, R.E., Lebonnois, S., Robertson, I.P., 2007b. Titan's corona: The contribution of exothermic chemistry. Icarus 191, 236–250.

Du, H., Hessler, J.P., Ogren, P.J., 1996. Recombination of methyl radicals. I. New data between 1175 and 1750 K in the falloff region. J. Phys. Chem. 100, 974–983.

Fenelly, J.A., Torr, D.G., 1992. Photoionization and photoabsorption cross sections of O, N_2, O_2 and N for aeronomic calculations. Atom. Data Nucl. Data Tables 51, 321–363.

Flasar, F.M., Achterberg, R.K., Conrath, B.J., Gierasch, P.J., Kunde, V.G., Nixon, C.A., Bjoraker, G.L., Jennings, D.E., Romani, P.N., Simon-Miller, A.A., Bézard, B., Coustenis, A., Irwin, P.G.J., Teanby, N.A., Brasunas, J., Pearl, J.C., Segura, M.E., Carlson, R.C., Mamoutkine, A., Schinder, P.J., Barucci, A., Courtin, R., Fouchet, T., Gautier, D., Lellouch, E., Marten, A., Prangé, R., Vinatier, S., Strobel, D.F., Calcutt, S.B., Read, P.L., Taylor, F.W., Bowles, N., Samuelson, R.E., Orton, G.S., Spilker, L.J., Owen, T.C., Spencer, J.R., Showalter, M.R., Ferrari, C., Abbas, M.M., Raulin, F., Edgington, S., Ade, P., Wishnow, E.H., 2005. Titan's atmospheric temperatures, winds, and composition. Science 308, 975–978.

Fox, J.L., Yelle, R.V., 1997. Hydrocarbon ions in the ionosphere of Titan. J. Geophys. Res. 24, 2179–2182.

Gan, L., 1991. Electron distributions and solar wind interaction with nonmagnetic planets. Ph.D. thesis, University of Michigan.

Gan, L., Keller, C.N., Cravens, T.E., 1992. Electrons in the ionosphere of Titan. J. Geophys. Res. 97, 12136–12151.

Halpern, J.B., Miller, G.E., Okabe, H., Nottingham, W., 1988. The UV photochemistry of cyanoacetylene. J. Photochem. Photobiol. A 42, 63–72.

Holland, D.M.P., Shaw, D.A., Hayes, M.A., Shpinkova, L.G., Rennie, E.E., Karlsson, L., Baltzer, P., Wannberg, B., 1997. A photoabsorption, photodissociation and photoelectron spectroscopy study of C_2H_4 and C_2D_4. J. Chem. Phys. 219, 91–116.

Hourdin, F., Talagrand, O., Sadourny, R., Courtin, R., Gautier, D., McKay, C.P., 1995. Numerical simulation of the general circulation of the atmosphere of Titan. Icarus 117, 358–374.

Hudson, R.D., 1971. Critical review of ultraviolet photoabsorption cross sections for molecules of astrophysical and aeronomical interest. Rev. Geophys. Space Phys. 9, 305–406.

Itikawa, Y., Hayashi, M., Ichimura, A., Onda, K., Sakimoto, K., Takayanagi, K., Nakamyura, M., Nishimura, H., Takayanagi, T., 1986. Cross sections for collisions of electrons and photons with nitrogen molecules. J. Phys. Chem. Ref. Data 15, 985–1010.

Janev, R.K., Reiter, D., 2004. Collision processes of $C_{2,3}H_y$ hydrocarbons with electrons and protons. Phys. Plasmas 11, 780–829.

Kameta, K., Machida, S., Kitajima, M., Ukai, M., Kouchi, N., Hatano, Y., Ito, K., 1996. Photoaborption, photoionization, and neutral-dissociation cross sections of C_2H_6 and C_3H_8 in the extreme-UV region. J. Electron Spectrosc. 79, 391–393.

Kella, D., Johnson, P.J., Pederson, H.B., Vejby-Christensen, L., Andersen, L.H., 1996. Dissociative recombination of N_2^+. Phys. Rev. Lett. 77. 2432.

Keller, C.N., Cravens, T.E., Gan, L., 1992. A model of the ionosphere of Titan. J. Geophys. Res. 97, 12117–12135.

Keller, C.N., Anicich, V.G., Cravens, T.E., 1998. Model of Titan's ionosphere with detailed hydrocarbon ion chemistry. Planet. Space Sci. 46, 1157–1174.

Kreile, J., Schweig, A., Thiel, W., 1982. Experimental and theoretical investigation of the photoionization of hydrogen cyanide. Chem. Phys. Lett. 87, 473–476.

Lara, L.M., Lellouch, E., Lopez-Moreno, J.J., Rodrigo, R., 1996. Vertical distribution of Titan's atmospheric neutral constituents. J. Geophys. Res. 101, 23261–23283.

Läuter, A., Lee, K.-S., Jung, K.-H., Vatsa, R.K., Mittal, J.P., Volpp, H.R., 2002. Absolute primary H atom quantum yield measurements in the 193.3 and 121.6 nm photodissociation of acetylene. Chem. Phys. Lett. 358, 314–319.

Lebonnois, S., 2000. Circulation générale et photochimie dans l'atmosphère de Titan. Ph.D. thesis, Université Toulouse III, Paul Sabatier.

Lebonnois, S., 2005. Benzene and aerosol production in Titan and Jupiter's atmospheres: A sensitivity study. Planet. Space Sci. 53, 486–497.

Lebonnois, S., Toublanc, D., Hourdin, F., Rannou, P., 2001. Seasonal variations of Titan's atmospheric composition. Icarus 152, 384–406.

Lebonnois, S., Bakes, E.L.O., McKay, C.P., 2003. Atomic and molecular hydrogen budget in Titan's atmosphere. Icarus 161, 474–485.

Lee, A.Y.T., Yung, Y.L., Moses, J., 2000. Photochemical modeling of CH_3 abundances in the outer Solar System. J. Geophys. Res. 105, 20207–20225.

Lehfaoui, L., Rebrion-Rowe, C., Laubé, S., Mitchell, J.B.A., Rowe, B.R., 1997. The dissociative recombination of hydrocarbon ions. I. Light alkanes. J. Chem. Phys. 106, 5406–5412.

Lellouch, E., Hunten, D.M., 1987. Titan atmosphere engineering model. Space Science Department Internal Publication ESLAB 87-199, ESA.

Lukirskii, A.P., Brytov, I.A., Zimkina, T.M., 1964. Photoionization absorption of He, Kr, Xe, CH_4, and methynal in the 23.6–250 Å region. Opt. Spectrosc. USSR, Engl. Transl. 17, 234.

Mason, E.A., Marrero, T.R., 1970. The diffusion of atoms and molecules. In: Bates, D.R., Estermann, I. (Eds.), Advances in Atomic and Molecular Physics, vol. 6. Academic Press, New York, pp. 155–232.

Mordaunt, D.H., Lambert, I.R., Morley, G.P., Arnold, M.N.R., Dixon, R.N., 1993. Primary product channels in the photodissociation of methane at 121.6 nm. J. Chem. Phys. 98, 2054–2065.

Mount, G.H., Moos, H.W., 1978. Photoabsorption cross sections of methane and ethane, 1380–1600 Å, at $T = 295$ K and $T = 200$ K. Astrophys. J. 224, L35–L38.

Mount, G.H., Warden, E.S., Moos, H.W., 1977. Photoabsorption cross sections of methane from 1400 to 1850 Å. Astrophys. J. 214, L47–L49.

Müller-Wodarg, I.C.F., Yelle, R.V., 2002. The effect of dynamics on the composition of Titan's upper atmosphere. J. Geophys. Res. 29, 54-1–54-4.

Müller-Wodarg, I.C.F., Yelle, R.V., Mendillo, M., Young, L.A., Aylward, A.D., 2000. The thermosphere of Titan simulated by a global three-dimensional time-dependent model. J. Geophys. Res. 105, 20833–20856.

Müller-Wodarg, I.C.F., Yelle, R.V., Mendillo, M., Aylward, A.D., 2003. On the global distribution of neutral gases in Titan's upper atmosphere and its effect on the thermal structure. J. Geophys. Res. 108, doi:10.1029/2003JA010054. 1453.

Müller-Wodarg, I.C.F., Yelle, R.V., Borggren, N., Waite Jr., J.H., 2006. Waves and horizontal structures in Titan's thermosphere. J. Geophys. Res. 111, doi:10.1029/2006JA011961. A12,315.

NOAA, online data, 2005. ftp://ftp.ngdc.noaa.gov/STP/SOLAR_DATA/SOLAR_RADIO/FLUX and http://www.sec.noaa.gov/ftpdir/weekly/Predict.txt.

Nuth, J.A., Glicker, S., 1982. The vacuum ultraviolet spectra of HCN, C_2N_2, and CH_3CN. J. Quant. Spectrosc. Radiat. Trans. 28, 223–231.

Okabe, H., 1981. Photochemistry of acetylene at 1470 Å. J. Chem. Phys. 75, 2772–2778.

Okabe, H., 1983. Photochemistry of acetylene at 1849 Å. J. Chem. Phys. 78, 1312–1317.

Orient, O.J., Srivastava, S.K., 1987. Electron impact ionization of H_2O, CO, CO_2, and CH_4. J. Phys. B 20, 3923–3936.

Richards, P.G., Fennelly, J.A., Torr, D.G., 1994. EUVAC: A solar EUV flux model for aeronomic calculations. J. Geophys. Res. 99, 8981–8992.

Romani, P.N., 1996. Recent rate constant and product measurements of the reactions $C_2H_3 + H_2$ and $C_2H_3 + H$—Importance for the photochemical modeling of hydrocarbons on Jupiter. Icarus 122, 233–241.

Schmitt, R.G., Brehm, R.K., 1966. Double beam spectrophotometry in the far ultraviolet. I. 1150 Å to 3600 Å. Appl. Opt. 5, 1111–1116.

Schunk, R.W., Nagy, A.F., 2000. Ionospheres: Physics, Plasma Physics, and Chemistry. Cambridge University Press, Cambridge.

Seki, K., Okabe, H., 1993. Photochemistry of acetylene at 193.3 nm. J. Phys. Chem. 97, 5284–5290.

Shah, M.B., Elliott, D.S., Gilbody, H.B., 1987. Pulsed crossed-beam study of the ionization of atomic hydrogen. J. Phys. B 20, 3501–3514.

Sheehan, C.H., St-Maurice, J.-P., 2004. Dissociative recombination of N_2^+, O_2^+, and NO^+: Rate coefficients for ground state and vibrationally excited ions. J. Geophys. Res. 109, doi:10.1029/2003JA010132.

Shemansky, D.E., Stewart, A.I.F., West, R.A., Esposito, L.W., Hallett, J.T., Liu, X., 2005. The Cassini UVIS stellar probe of the Titan atmosphere. Science 308, 978–982.

Slagle, I.R., Gutman, D., Davies, J.W., Pilling, M., 1988. Study of the recombination reaction $CH_3 + CH_3 \rightarrow C_2H_6$. I. Experiment. J. Phys. Chem. 92, 2455–2462.

Smith, G.R., Strobel, D.F., Broadfoot, A.L., Sandel, B.R., Shemansky, D.E., Holdberg, J.B., 1982. Titan's upper atmosphere: Composition and temperature form the EUV solar occultation results. J. Geophys. Res. 87, 1351–1359.

Smith, N.S., Raulin, F., 1999. Modeling of methane photolysis in the reducing atmospheres of the outer Solar System. J. Geophys. Res. 104, 1873–1876.

Stolte, W.C., He, Z.X., Cutler, J.N., Lu, Y., Samson, J.A.R., 1998. Dissociative photoionization cross sections of N_2 and O_2 from 100 to 800 eV. Atom. Data Nucl. Data Tables 69, 171–179.

Strobel, D.F., Summers, M.E., Zhu, X., 1992. Titan's upper atmosphere: Structure and ultraviolet emissions. Icarus 100, 512–526.

Tian, C., Vidal, C.R., 1998a. Cross sections of electron impact ionization of ethylene. Chem. Phys. Lett. 288, 499–503.

Tian, C., Vidal, C.R., 1998b. Electron impact dissociative ionization of ethane: Cross sections, appearance potentials, and dissociative pathways. J. Chem. Phys. 109, 1704–1712.

Tobiska, W.K., Barth, C.A., 1990. A solar EUV flux model. J. Geophys. Res. 95, 8243–8251.

Toublanc, D., Parisot, J.P., Brillet, J., Gautier, D., Raulin, F., McKay, C.P., 1995. Photochemical modeling of Titan's atmosphere. Icarus 113, 2–26.

Vervack Jr., R.J., Sandel, B.R., Strobel, D.F., 2004. New perspectives on Titan's upper atmosphere from a reanalysis of the Voyager 1 UVS solar occultations. Icarus 170, 91–112.

Vuitton, V., Yelle, R., 2005. Ethane chemistry on Titan. In: Proceedings of the Titan/Cassini–Huygens Meeting, Crete, Greece.

Vuitton, V., Doussin, J.-F., Benilan, Y., Raulin, F., Gazeau, M.-C., 2006a. Experimental and theoretical study of hydrocarbon photochemistry applied to Titan stratosphere. Icarus 185, 287–300.

Vuitton, V., Yelle, R.V., Anicich, V.G., 2006b. The nitrogen chemistry of Titan's upper atmosphere revealed. Astrophys. J. 647, L175–L178.

Wahlund, J.-E., Boström, R., Gustafsson, G., Gurnett, D.A., Kurth, W.S., Pedersen, A., Averkamp, T.F., Hospodarsky, G.B., Persoon, A.M., Canu, P., Neubauer, F.M., Dougherty, M.K., Eriksson, A.I., Morooka, M.W., Gill, R., André, M., Eliasson, L., Müller-Wodarg, I., 2005. Cassini measurements of cold plasma in the ionosphere of Titan. Science 308, 986–989.

Waite Jr., J.H., Niemann, H., Yelle, R.V., Kasprzak, W.T., Cravens, T.E., Luhmann, J.G., McNutt, R.L., Ip, W.-H., Gell, D., De La Haye, V., Müller-Wordag, I., Magee, B., Borggren, N., Ledvina, S., Fletcher, G., Walter, E., Miller, R., Scherer, S., Thorpe, R., Xu, J., Block, B., Arnett, K., 2005. Ion neutral mass spectrometer results from the first flyby of Titan. Science 308, 982–986.

Wakeham, W.A., Slater, D.H., 1973. Diffusion coefficients for *n*-alkanes in binary gaseous mixtures with nitrogen. J. Phys. B At. Mol. Phys. 6, 886–896.

Wilke, C.R., 1950. Diffusional properties of multicomponent gases. Chem. Eng. Prog. 46, 95–104.

Wilson, E.H., 2002. Investigations into the photochemistry of the current and primordial atmosphere of Titan. Ph.D. thesis, University of Michigan.

Wilson, E.H., Atreya, S.K., 1999. Sensitivity studies of methane photolysis and its impact on hydrocarbon chemistry in the atmosphere of Titan. Bull. Am. Astron. Soc. 31. 1142.

Wilson, E.H., Atreya, S.K., 2004. Current state of modeling the photochemistry of Titan's mutually dependent atmosphere and ionosphere. J. Geophys. Res. 109, doi:10.1029/2003JE002181.

Wu, C.Y.R., Judge, D.L., 1985. Photoabsorption cross section of acetylene in the EUV region. J. Chem. Phys. 82, 4495–4499.

Wu, C.Y.R., Chen, F.Z., Judge, D.L., 2001. Measurements of temperature-dependent absorption cross sections of C_2H_2 in the VUV–UV region. J. Geophys. Res. 106, 7629–7636.

Yelle, R.V., Strobel, D.F., Lellouch, E., Gautier, D., 1997. Engineering models for Titan's atmosphere. ESA Spec. Publ. 1177, 243–256.

Yelle, R.V., Borggren, N., De La Haye, V., Kasprzak, W.T., Niemann, H.B., Müller-Wodarg, I., Waite Jr., J.H., 2006. The vertical structure of Titan's upper atmosphere from Cassini ion neutral mass spectrometer measurements. Icarus 182, 567–576.

Yung, Y.L., 1987. An update of nitrile photochemistry on Titan. Icarus 72, 468–472.

Yung, Y.L., Allen, M., Pinto, J.P., 1984. Photochemistry of the atmosphere of Titan: Comparison between model and observations. Astrophys. J. Suppl. Ser. 55, 465–506.

Zelikoff, M., Wanabee, K., 1953. Absorption coefficients of ethylene in the vacuum ultraviolet. J. Opt. Soc. Am. 43, 756–759.

Zheng, S.H., Srivastava, S.K., 1996. Electron-impact ionization and dissociative ionization of acetylene. J. Phys. B At. Mol. Opt. Phys. 29, 3235–3244.

Zipf, E.C., Espy, P.J., Boyle, C.F., 1980. The excitation and collisional deactivation of metastable $N(^2P)$ atoms in auroras. J. Geophys. Res. 85, 687–694.